



## DESIGN OF AN ASYMMETRIC DIRECTIONAL COUPLER COMBINING SILICON AND SILICON NITRIDE

**Alejandro Santomé Valverde**

**Supervisor: Pablo Sanchis Kilders**

**Co-supervisor: Jorge Parra Gómez**

Master's Thesis presented at Escuela Técnica Superior de Ingeniería de Telecomunicación of Universitat Politècnica de València, to obtain the title "Máster en Ingeniería de Telecomunicación".

Course 2020-21

Valencia, 12 September 2021



## Resumen

El objetivo del trabajo fin de máster es llevar a cabo el diseño de un acoplador direccional asimétrico en tecnología fotónica de silicio y nitruro de silicio. Dicha configuración ayudaría a mejorar la eficiencia de conmutación en estructuras híbridas formadas por silicio y nuevos materiales. En este trabajo, el diseño se particularizará para estructuras híbridas formadas por silicio, nitruro de silicio y materiales de cambio de fase. La incorporación de guías de nitruro de silicio permite inyectar señales ópticas de alta potencia sin que éstas se vean afectadas por el efecto no-lineal TPA presente en silicio. Dichas señales de alta potencia son necesarias para cambiar las propiedades ópticas de los materiales de cambio de fase y de esta forma conseguir conmutación fotónica.

## Resum

L'objectiu del treball fi de màster és dur a terme el disseny d'un acoblador direccional asimètric en tecnologia fotònica de silici i nitruro de silici. Aquesta configuració ajudaria a millorar l'eficiència de commutació en estructures híbrides formades per silici i nous materials. En aquest treball, el disseny es particularitzarà per a estructures híbrides formades per silici i materials de canvi de fase. La incorporació de guies de nitruro de silici permet inyectar senyals òptics d'alta potència sense que aquestos es vegin afectats per l'efecte no-lineal TPA present en el silici. Aquestos senyals d'alta potència són necessaris per canviar les propietats òptiques dels materials de canvi de fase i d'aquesta manera aconseguir commutació fotònica.

## Abstract

The objective of the master's thesis is to carry out the design of an asymmetric directional coupler in silicon and silicon nitride photonic technology. Such a configuration would help to improve the switching efficiency in hybrid structures formed by silicon and new materials. In this work, the design will be particularized for hybrid structures formed by silicon and phase change materials. The incorporation of silicon nitride guides allows to inject high power optical signals without them being affected by the non-linear TPA effect present in silicon. Such high-power signals are necessary to change the optical properties of phase change materials and thus achieve photonic switching.



## Table of contents

Chapter 1.	Introduction and review of the technology.....	2
1.1	Silicon-based integrated photonics.....	2
1.1.1	Introduction to silicon photonics.....	2
1.1.2	Current status and application areas of silicon photonics .....	4
1.2	Silicon nitride technology .....	5
1.2.1	Material properties .....	5
1.2.2	Photonic devices and applications.....	7
1.2.3	Silicon nitride platforms.....	8
1.3	Integration of new materials in silicon technology. ....	9
1.3.1	Phase change materials.....	9
1.4	Review of types of directional couplers. ....	11
1.4.1	Silicon directional couplers.....	11
1.4.2	Asymmetric directional couplers.....	12
1.4.3	Directional couplers combining more than one material .....	14
Chapter 2.	Objectives, motivation and methodology.....	15
2.1	Objectives.....	15
2.2	Description and motivation of the device to be designed.....	15
2.3	Methodology and design tools .....	17
Chapter 3.	Modal analysis of the waveguides of the directional coupler .....	18
3.1	Modal analysis of the silicon waveguide .....	18
3.2	Modal analysis of the silicon nitride waveguide .....	20
Chapter 4.	Design of the asymmetric directional coupler.....	23
4.1	Design parameters. Influence on the performance and limitations. ....	23
4.1.1	Influence of the design parameters.....	23
4.1.2	Limitations .....	23
4.2	Analysis of the configurations available .....	23
4.2.1	Supermodes .....	23
4.2.2	BeamPROP simulation.....	27
4.2.3	Addition of the GST .....	30
4.3	Optimal design parameters.....	31
4.4	Possible configurations for a new the asymmetric directional coupler .....	32
Chapter 5.	Conclusions and future work.....	35
5.1	Conclusions .....	35
5.2	Future work .....	35

## Chapter 1. Introduction and review of the technology

Photonics defines both the physical science and the application of light (photons) in terms of generation, detection, and manipulation by means of transmission, emission, modulation, switching, amplification, signal processing and sensing. Photonics increased its popularity when optical telecommunication systems appeared, enabling the possibility of guiding signals over optical transmission lines instead of coaxial cables or copper wire pairs. This was made possible for two reasons. The invention of first practical semiconductor light emitters in the early 1960s, together with the development of optical fibres in the 1970s, converted photonics as a powerful solution. After that moment, some tasks that were previously performed by electronics started to be carried out through photonic systems.

Photonics technology includes emitters (light sources, such as lasers or LEDs), waveguides and some other opto-electronic devices that encode digital information onto optical signals and make the conversion between optical signals to electrical ones. Despite the optical components are discrete for a large number of applications, to carry out some other tasks a direct coupling between components is required. Therefore, a new branch of photonics called integrated photonics has emerged as a solution for these kinds of applications, where all the components (e.g., waveguides, interferometers, splitters...) are integrated on a common planar substrate [1][2].

The miniaturization of components is one of the pursued goals for integrated photonics. Following the same criteria employed in electronics, the designers try to allocate the highest number of components in the chip. However, the integration density in photonic integrated circuits (PICs) is far from the values used in electronics nowadays [3]. Meanwhile a new electronic integrated circuit contains about a billion transistors, the number of devices in a PIC can oscillate from hundreds to thousands. To overcome this backlog in terms of density, researchers have been studying different properties of the materials employed to fabricate PICs. The high wavelength of light, combined with high-index materials, allows the development of micron-size photonic devices [4]. Furthermore, considering the influence of the refractive index, there is a type of materials that are at the forefront due to the large variation of their indices, the phase change materials.

### 1.1 Silicon-based integrated photonics

#### 1.1.1 Introduction to silicon photonics

Silicon photonics is the most used platform to develop photonic integrated circuits. The reason behind is that silicon is not only interesting in terms of cost but also in technology. It is well-known that wafers made of silicon or Silicon-on-Insulator (SOI) are much cheaper than the ones made with combinations of III-V materials. Gallium arsenide (GaAs), indium phosphide (InP) or lithium niobate (LiNbO<sub>3</sub>) are more expensive than silicon. However, depending on the application, these materials could be necessary. For example, to create modulators the LiNbO<sub>3</sub> is the most employed, whereas lasers and photodetectors are mainly made of InP or GaAs [5].

The problem with the materials mentioned before is that they are not easy to integrate all together in the same photonic integrated circuit. Thus, silicon-based designs are being intensively researched because they have important advantages over other substrates. One of these characteristics is the high index contrast between silicon (Si) and its oxide ( $\text{SiO}_2$  or silica), that enables the miniaturization of components. Furthermore, the generation of structures with these materials is quite cheap, which is one of the pursued goals mentioned. However, the most interesting property for designers is that Si (and SOI) are compatible with CMOS technology, that is widely used in electronics. If the electronic and the photonic components in the chip are silicon-based it would be possible to fabricate devices with submicron dimensions and reaching values of bending radius in the order of micrometers.

Optical communications are the main application of silicon photonics since the first product was released. It was made by a UK-based manufacturer called Bookham Technology Ltd in 1998. Before that, they were researching for a decade about the development of PICs using SOI wafers [6]. The aim was finding a guiding structure that was single mode, producible using conventional processes and polarization independent. During this process they developed test products like the passive optical network (PON) transceiver shown in Fig. 1.

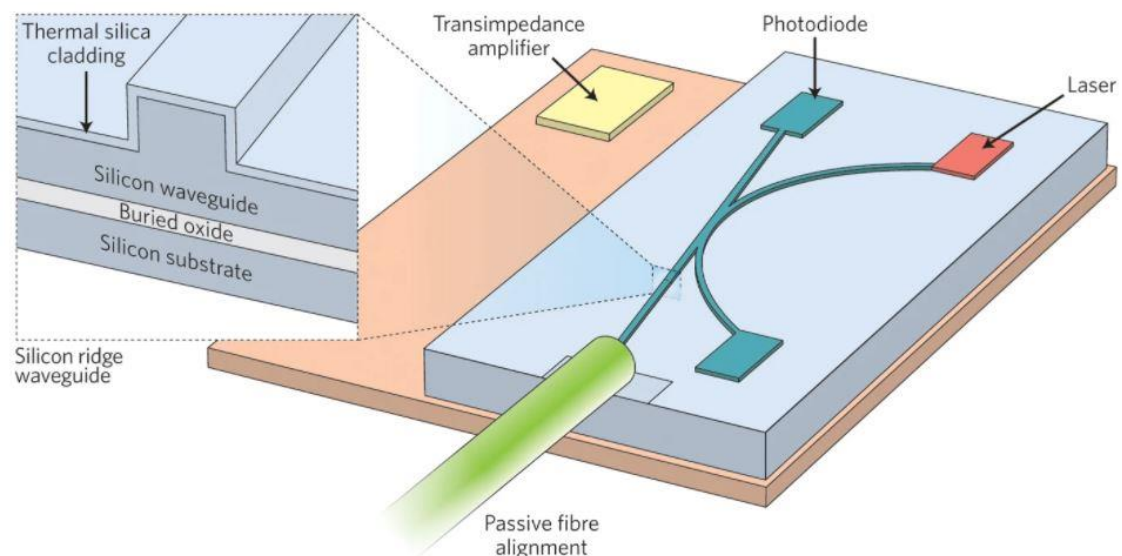


Fig. 1. PON transceiver made by Bookham in 1993 [6].

The inclusion of Intel and IBM in the silicon photonics market increased the interest in the field. Nevertheless, the leading of commercial silicon-based photonic products (revenue, gross margins and shipped channels) was Kotura Inc. The company, which was acquired in 2013 by Mellanox Technologies Ltd., was the second step of Andrew Rickman, founder of Bookham. Kotura believed that with the growth of internet traffic in the foreseeable future, optical communications and silicon photonics would play a major role in the technology. Specifically, in data centers, due to the possible advantages in terms of power consumption, operation costs, latency or even cable densities. Now it is reasonable to say the assumptions they made were in the right direction.

Despite being one of the most powerful platforms, silicon has some disadvantages. One of the important shortcomings that designers have to face is that light generation at any band is still not achieved [7] due to the non-active properties of silicon. Furthermore, light detection in the telecommunication band is also a problem, apart from the well-known non-linearities, such as the lack of second-order optical nonlinearity (desired for modulation), and the nonlinear absorptions when its third-order optical nonlinearity is exploited [8]. In spite of the issues mentioned above, it has been proposed the possibility of achieving light emission by using third harmonic generation [9], but it has been only tested in controlled environments and they still could not prove that behaviour in practical environments.

On the other hand, for applications where data storage is required, the volatility of silicon can be not appropriate. Fortunately, silicon can be combined with other non-volatile materials creating hybrid structures that can be employed, for example, to create optical memories [10][11].

Considering all the points listed in Table 1, silicon photonics is a powerful platform that will be core in the upcoming telecommunication systems.

Advantages	Drawbacks
CMOS compatibility	Lack of light generation
Low cost	Lack of electro-optic effect
Transparent to light in telecommunication wavelengths	Difficult coupling to fibres
High refractive index contrast	Volatile switching response

Table 1. Advantages and disadvantages of silicon photonics platform.

### 1.1.2 Current status and application areas of silicon photonics

Many different applications can be carried out using silicon photonics. Apart from the transceivers market for datacentres, which is currently the main area of silicon photonics (\$84M in 2020), other interesting applications have already started to develop their systems by using this platform. It is the case of Genalyte, a California company who released systems for immunoassays based on silicon photonics elements in 2020. Another example is KVH, who had released fiber optical gyroscopes (FOG) for robotic car navigation [12], or Aeva, other California-based company developing frequency modulated continuous wave (FMCW) LiDAR with silicon photonics to serve autonomous driving. From electronic noses, through optical coherence tomography or cardiovascular diagnostic devices, silicon photonics demonstrates its potential for many applications. Moreover, hot topics such as neuromorphic computing and quantum processing could also benefit from the platform.

Compound annual growth rate (CAGR) of some of the applications mentioned before is shown in Fig. 2. These results obtained by Yole Développement present an analysis of silicon photonics market up to 2026 in terms of revenues, averaging price sales and volumes segmented by applications and technologies. They estimate a stunning average CAGR of 49% from 2021 to 2026.

### 2020-2026 silicon photonics die forecast by application

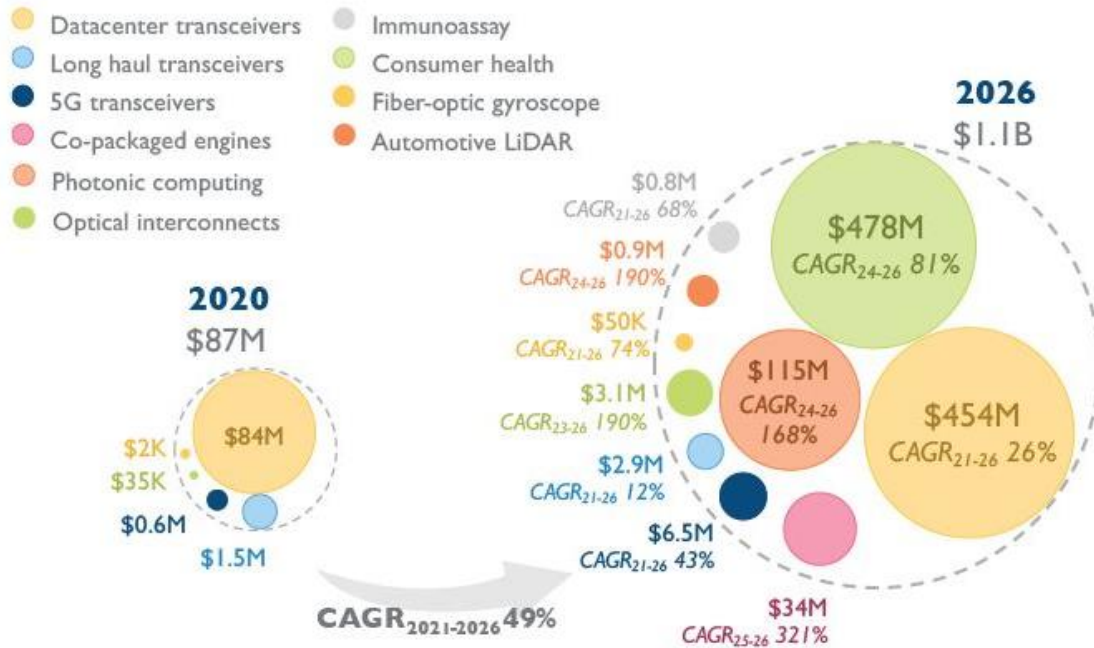


Fig. 2. Forecast of silicon photonics from 2020 to 2026 [12].

## 1.2 Silicon nitride technology

### 1.2.1 Material properties

Silicon nitride ( $\text{Si}_3\text{N}_4$ ) is a common material in CMOS fabs. It has a refractive index around 2 at telecommunication wavelengths in third window (1550 nm), thus if it is surrounded by silica (~1.5) the core-cladding variation in terms of refractive index is not as high as SOI. This seems to be a drawback because with high index contrast it is possible to create devices with smaller footprints. However, high contrast also makes the waveguide prone to scattering losses due to nm-scale roughness of the sidewalls of the waveguide and, furthermore, the sensitivity of the effective index to the waveguide width is high. It also leads to less-than-ideal crosstalk in arrayed waveguide gratings. In silicon nitride waveguides these conditions are relaxed to a certain degree, meanwhile the small footprint is maintained [13].

Comparing silicon nitride wafers with SOI wafers there are some key points to determine which is the correct material depending on the desired properties. These characteristics could be the mentioned index contrast, apart from transparency range, the manufacturing flexibility, or the non-linear behaviour of each material. In terms of transparency range, SOI is not appropriate for applications where the wavelength is shorter than 1.1  $\mu\text{m}$  due to their absorption losses [14]. On the other hand, silicon nitride is transparent throughout almost all of the visible range, thus is a powerful solution for designs with wavelengths below that value.

Regarding to the third order nonlinearity, Kerr nonlinearity is not useful in silicon in the range of 1300-1500 nm due to the two-photon absorption (TPA) [15]. Meanwhile, the Kerr nonlinearity is weaker in silicon nitride, but the two-photon absorption is nearly zero. Thus, SiN can be employed in that range for applications where the third order nonlinearity is exploited [13].

Another interesting property is the second order nonlinearity and Pockels effect. It is true that they are negligible for both Si and SiN, which means that electro-optic modulation is not possible for them. For Silicon-on-Insulator there is the option of using the free carrier induced electro-refraction. However, the resulting modulators are large (in the order of mm) and they are limited for achieving ultra-fast modulation speeds. Recently some researchers reported strong electro-refraction in SOI waveguides in which a strain gradient was induced using a strained SiN overlayer. They are still discussing the precise mechanism of that design, but some of them attribute the phenomenon to a strain gradient in the silicon nitride and not in the silicon, which could enable the possibility of create strained SiN-based Pockels modulators [16].

Finally, another advantage that silicon nitride has is the low loss behaviour. SOI waveguides surrounded by silica have a typical value of losses between 1 and 2 dB/cm. This is related with the roughness of the sidewalls of the material. In silicon nitride waveguides these losses can be, theoretically, reduced up to an order of magnitude lower. Therefore, SiN may be more suitable for applications where the losses are critical.

The graph shown in Fig. 3 depicts some of the characteristics mentioned above for the reported values of SOI and silicon nitride waveguides, while Table 2 lists these advantages of silicon nitride for photonics.

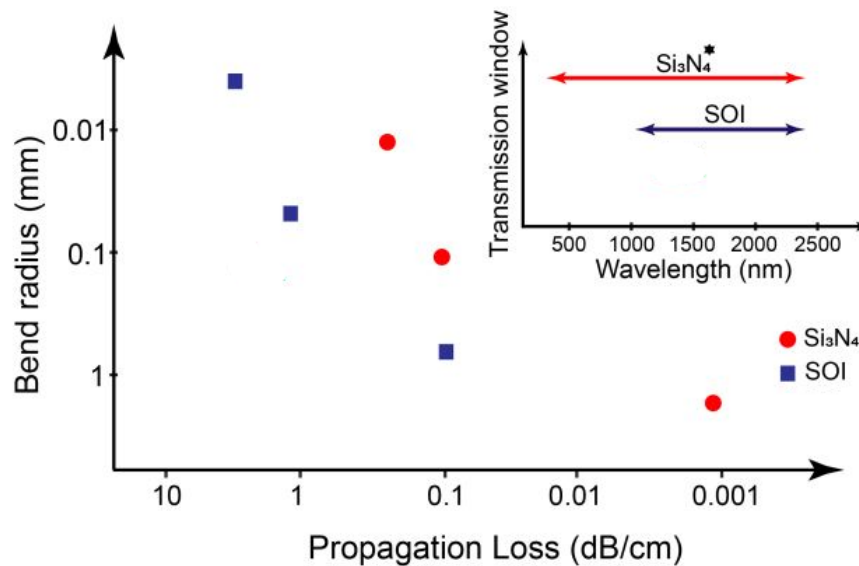


Fig. 3. Bend radius, propagation loss, and window of transparency for SiN and SOI waveguides [17].

Advantages of silicon nitride
Transparency for visible and near-infrared wavelengths
Compatible with CMOS technology
Photonic waveguide with lower propagation losses
Low-temperature sensitivity
Custom-manufacturing flexibility

Table 2. Advantages of silicon nitride photonics.

### 1.2.2 Photonic devices and applications

Several devices have been implemented using silicon nitride technology for optical communications. They can be categorized as passive, such as splitters, demultiplexers, resonators, grating couplers; or active, such as modulators [18]. Some examples of these devices are depicted in Fig. 4. At the top left in Fig. 4(a) it is shown a bi-layer grating coupler [19] on the SiN-on-SOI platform by using the principle demonstrated in [20]. Fig. 4(b) shows a polarization rotator from/to TE and TM polarization, where they report a conversion efficiency of 97% by using Si<sub>3</sub>N<sub>4</sub>-on-SOI platform. Last example is the polarization beam splitter presented in Fig. 4(c)[21].

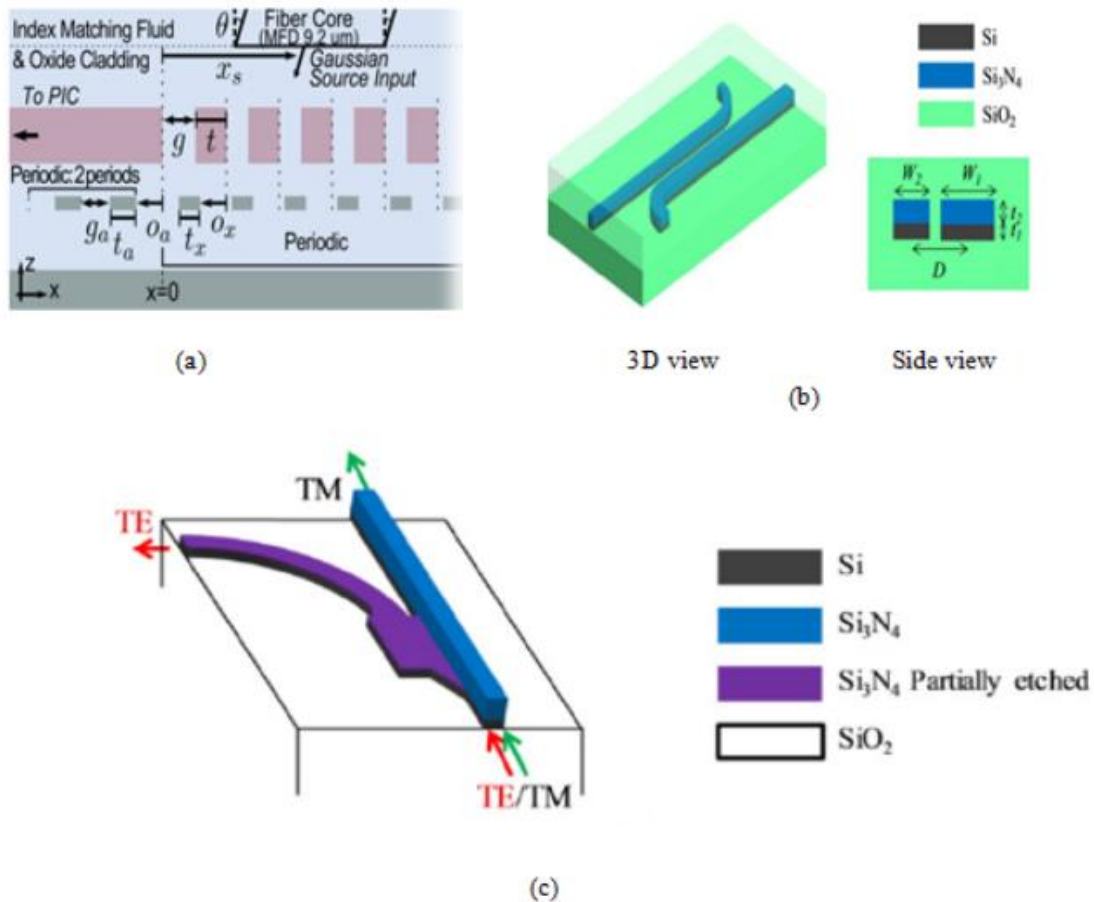
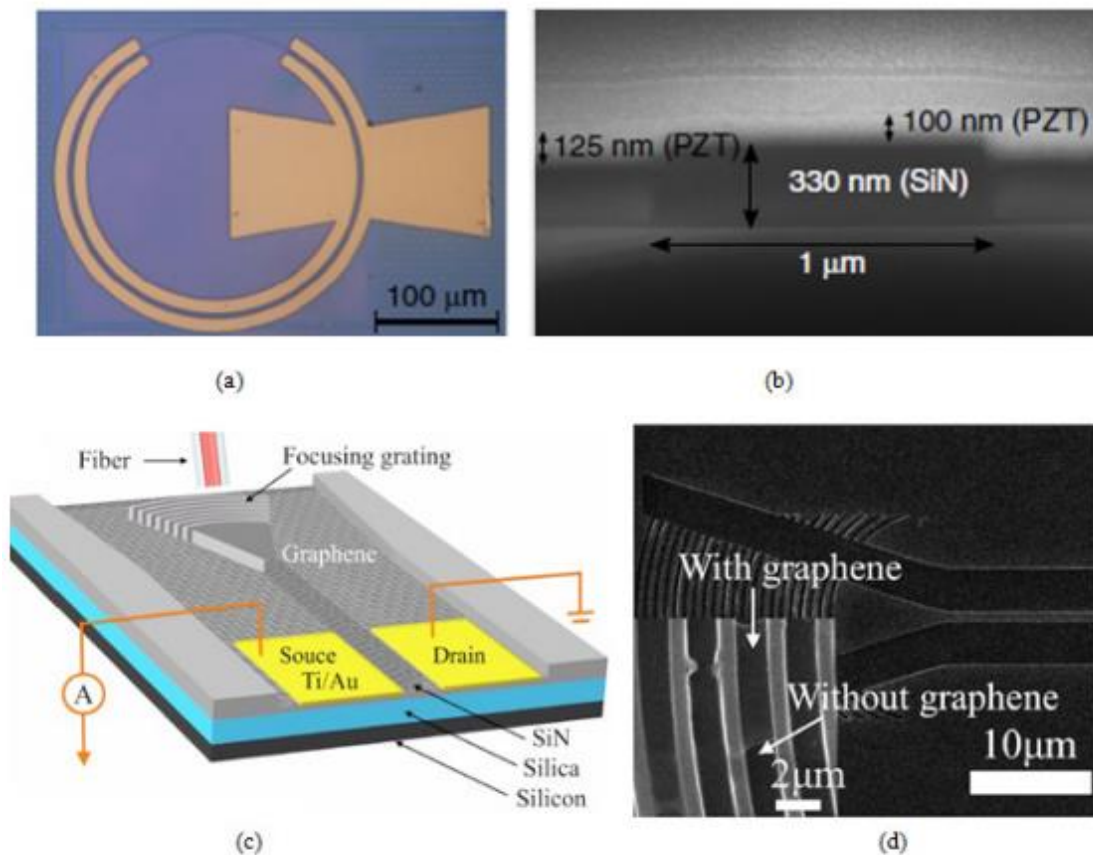


Fig. 4. Si<sub>3</sub>N<sub>4</sub> based passive devices [18]. (a) Side view of a bi-layer grating coupler. (b) Polarization rotator. (c) Polarization beam splitter from [21].

Regarding the active photonic integrated circuits, silicon nitride platform has been used to develop high-speed modulators in both O and C band, as depicted in Fig. 5(a) and Fig. 5(b); or photodetectors (PDs), as shown in Fig. 5(c) and Fig. 5(d), where it is used a graphene-based photodetector integrated on the Si<sub>3</sub>N<sub>4</sub> ridge waveguide, as demonstrated in [22]. SiN can be also employed for more complex applications like spectroscopic sensing [23], or lasers [24].



**Fig. 5.** Si<sub>3</sub>N<sub>4</sub> based active devices [18]. (a) Microscopic image of a microring modulator. (b) SEM image of a PZT-covered SiN waveguide. (c) Photodetector with graphene on the SiN waveguide. (d) SEM image of areas with and without graphene.

### 1.2.3 Silicon nitride platforms

Silicon nitride market is projected to grow from 90M USD in 2018 to 127M USD in the year 2023, at a CAGR of 7.2%, as published in MarketsAndMarkets report in May 2019. The interesting properties make silicon nitride a suitable material for use in end-use industries such as automotive, aerospace, solar photovoltaic, biophotonics, tele/datacom, optical signal processing and sensing, and medical among.

In the field of photonics, multiple commercial foundry platforms have evolved including IBM-CNM together with VLC Photonics, apart from LioniX's TriPleX, IMECs BioPIX or Ligentec's Damascene processes. They use Low-pressure chemical vapor deposition (LPCVD) nitride in order to keep the process in the CMOS line, taking advantage of the compatibility mentioned before.

Nowadays manufacturers use three types of waveguides with variations in core geometry and fabrication process, as it is shown in Fig. 6. The single and double strip geometries are part of the TriPleX foundry platform [25], while the buried designs are part of the TriPleX and Photonic Damascene processes.

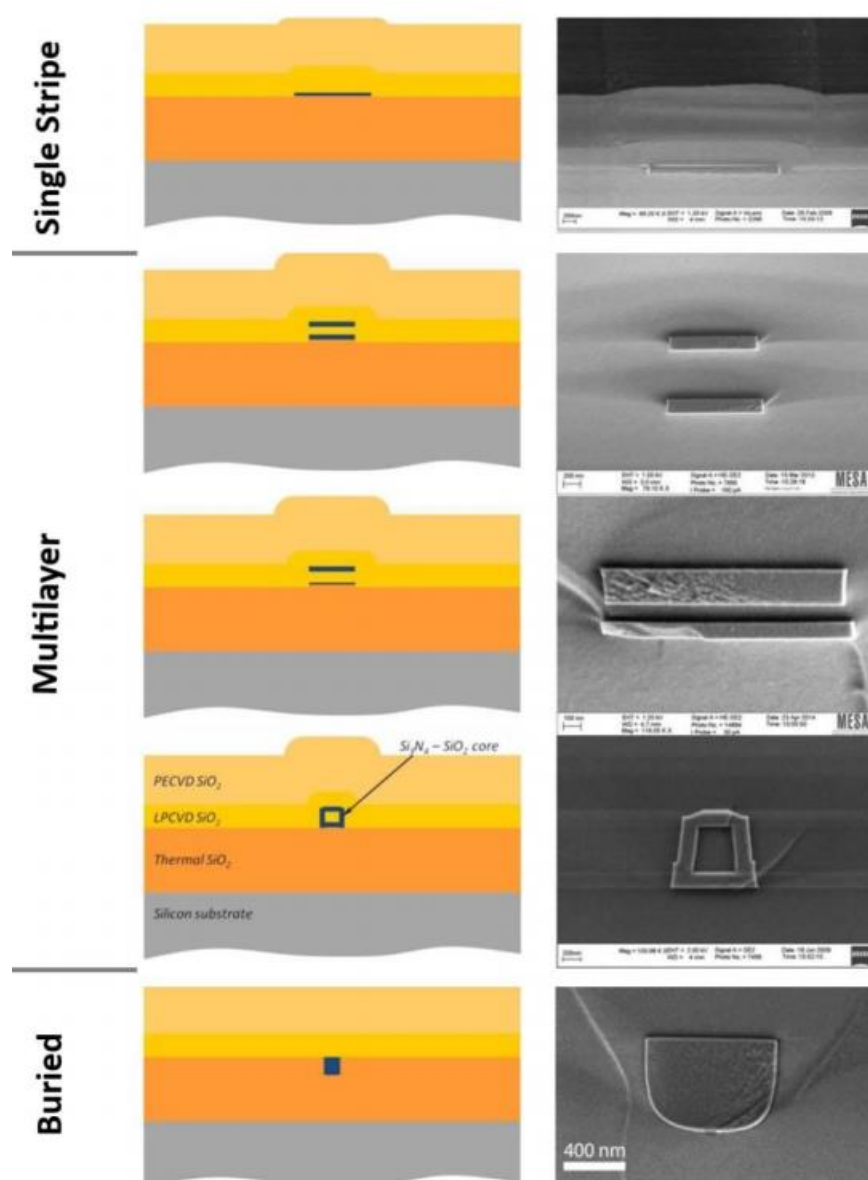


Fig. 6.  $\text{Si}_3\text{N}_4$  waveguide types, cross sections and SEM photographs [17].

### 1.3 Integration of new materials in silicon technology.

#### 1.3.1 Phase change materials

As it was mentioned in section 1.1.1, silicon has some drawbacks that can be minimized by its combination with other materials. In the last years, researchers have demonstrated devices based on phase change materials (PCMs) for several applications, such as routing [26] or switching [27]. The reason is that the phase transition in phase change materials creates a big change in the refractive index (index change  $> 1$ ), generating an optical modulation that allows the construction of compact device architectures.

Materials such as germanium-antimony-tellurides ( $\text{Ge}_2\text{Sb}_2\text{Se}_4\text{Te}_1$  (GSST) or  $\text{Ge}_2\text{Sb}_2\text{Te}_5$  (GST)) have been exploited to create phase-change memories [11][12], taking advantage of the non-volatile response of these chalcogenide materials. Another promising phase change material is vanadium dioxide ( $\text{VO}_2$ ) due to the large change of refractive index between its metallic and

insulating state. By using this property it is possible to create switches, such as the one shown in Fig. 7(a)[30] or [31]; optical modulators (Fig. 7(b)[26] or [32]); or photodetectors [33].

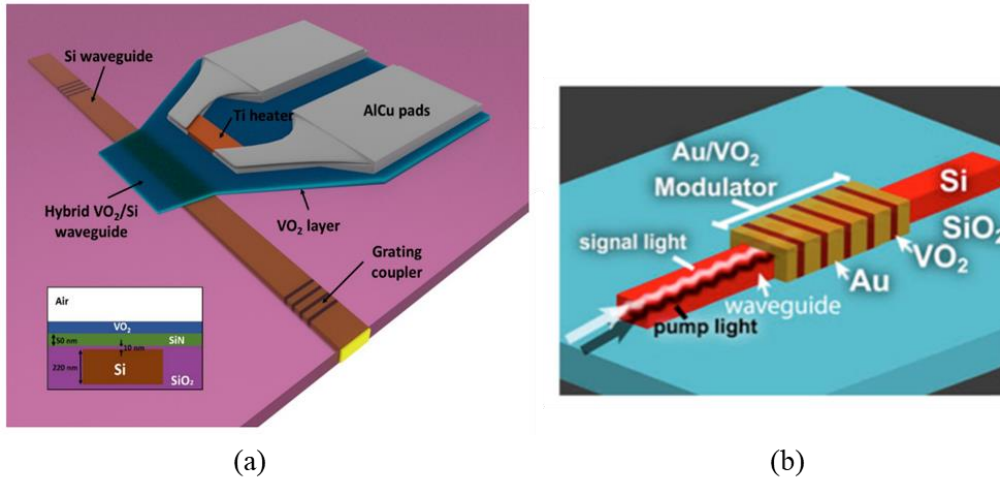


Fig. 7. (a) Hybrid VO<sub>2</sub>/Si waveguide with a lateral Ti microheater[30]. (b) Si/Au/VO<sub>2</sub> all-optical modulator [26].

Among the phase change materials mentioned, GST stands out due to its singular attributes in terms of refractive index variation and non-volatility. GST presents a huge change in the refractive index for telecommunication wavelengths [28] both in real and imaginary components. Taking advantage of this property, designers can develop ultra-compact high-performance optical switches which can be either triggered electrically or optically. By injecting an in-plane optical pulse it is possible to change the material from amorphous to crystalline and vice versa in hybrid Si/GST structures, where the active material is the GST [34]. Fig. 8 shows this behaviour, obtaining extinction ratios around 10 dB for multiple switching cycles, where more than one in-plane pulse is needed to induce the change in the material.

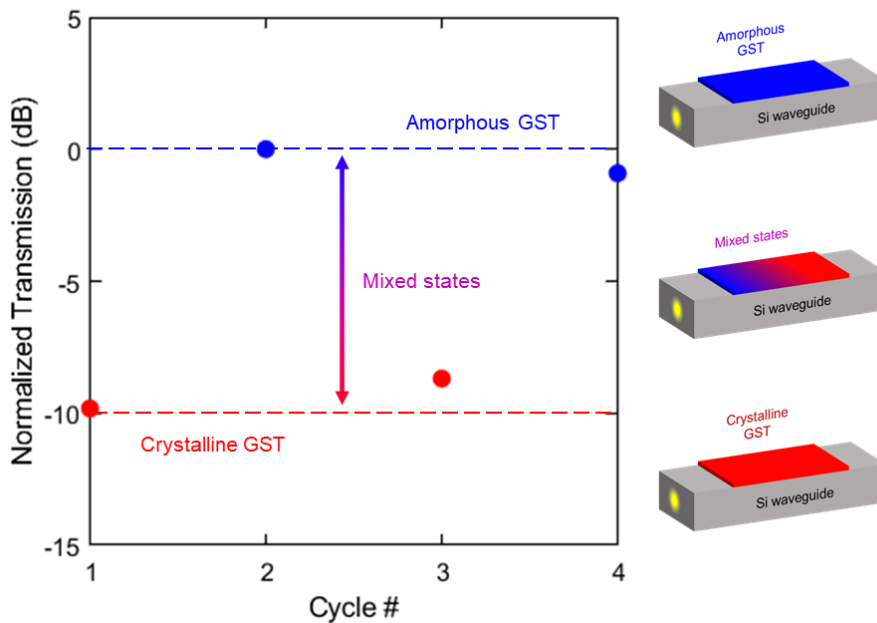


Fig. 8. Four all-optical switching cycles in a hybrid Silicon-GST waveguide. [34]

## 1.4 Review of types of directional couplers.

### 1.4.1 Silicon directional couplers

Silicon and SOI directional couplers are widely used in photonics for routing, phase control, 3 dB power splitters, combiners, multiplexers and demultiplexers, optical filters or switches. The working principle behind them is that a coupling section appears where a periodic tower exchange occurs between two photonic waveguides placed closes together. There are different theories to model the performance: the coupled mode theory and the supermodes theory. In this work, the theory employed to design the directional couplers is the second one, where the two coupler waveguides are regarded as one waveguide. This means that two supermodes appear, the odd mode and the even mode, represented in Fig. 9.

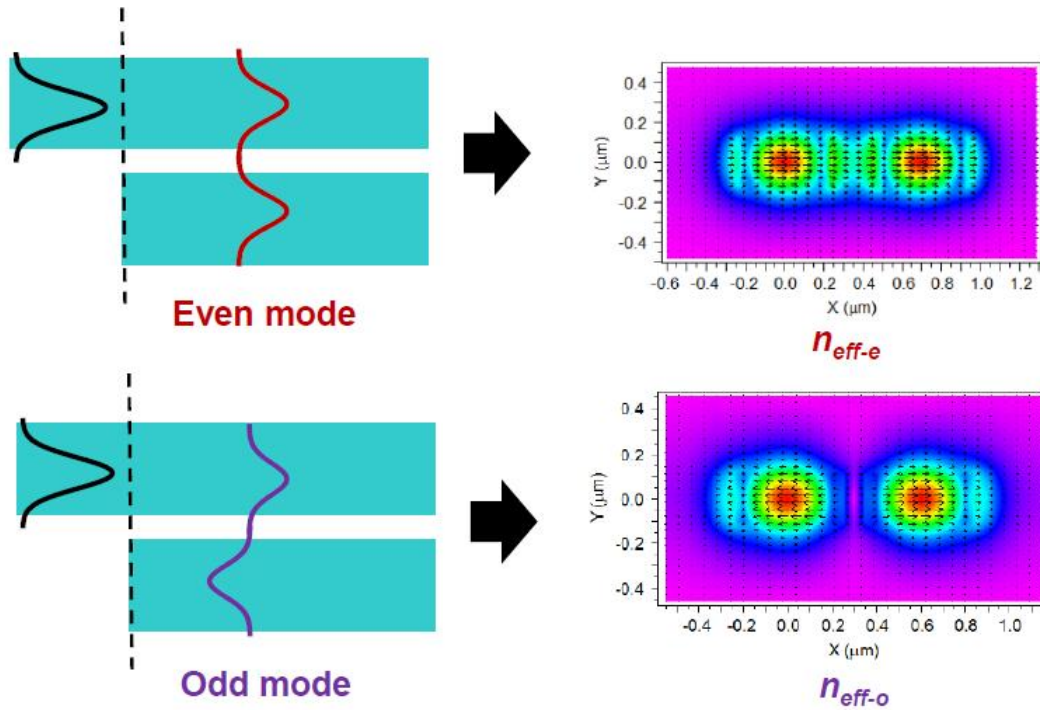


Fig. 9. Even mode and odd mode of supermodes theory [35].

In this situation it is possible to define the beat length ( $L_B$ ) as it is shown in equation (1).

$$L_B = \frac{\lambda}{|n_{eff-e} - n_{eff-o}|} \quad (1)$$

The design parameters that a designer can vary to create a symmetric directional coupler are the waveguide separation ( $s$ ), which determines the  $L_B$ ; and the waveguide length ( $L$ ), which determines the power at the output ports, as it is shown in Fig. 10 ( $K$  is the coupling coefficient, defined by equation (2)).

$$K = \sin^2\left(\frac{\pi L}{L_B}\right), \quad 0 \leq K \leq 1 \quad (2)$$

For lower separations, the coupling will be stronger and, therefore, the directional couplers will be shorter. Furthermore, the bandwidth of the directional couplers will be also separation dependent. For closes waveguides, the optical bandwidth will be broader.

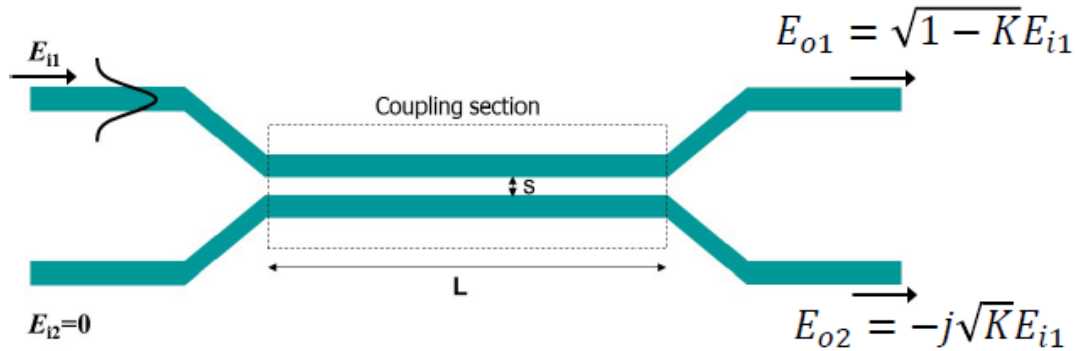


Fig. 10. Design parameters of a directional coupler [35].

Fig. 11 depicts an example of a directional coupler working as a polarization splitter [36]. Fig. 11(a) shows the schematic layout of the polarization splitter, while Fig. 11(b) and Fig. 11(c) represent the TE and TM modes, respectively.

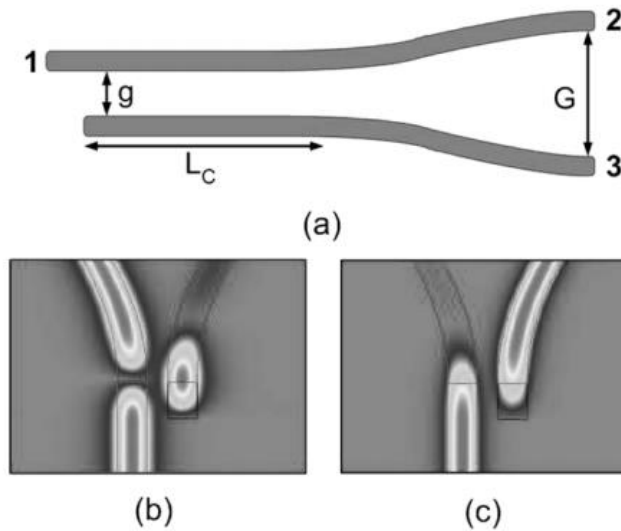


Fig. 11. Compact Silicon-on-Insulator polarization splitter [36].

#### 1.4.2 Asymmetric directional couplers

Despite the most common directional couplers are symmetric, there is the possibility to modify the waveguides to obtain the desired performance depending on the application. As it is shown in Fig. 12, it is possible to combine symmetric and asymmetric sections in the couplers in order to control the phase of the signal [37]. In this design, when the light propagates through the symmetric waveguide, it will work like the traditional directional coupler. However, in the asymmetric-waveguide-based phase control section, the light propagates without coupling, but it will be phase-shifted relative to the light in the other waveguide. Then, the light couples again in the symmetric directional coupler, obtaining a small phase shift between the two symmetric couplers. With this design it is possible to compensate the phase shift for the wavelength-dependent coupling ratios of the traditional couplers.

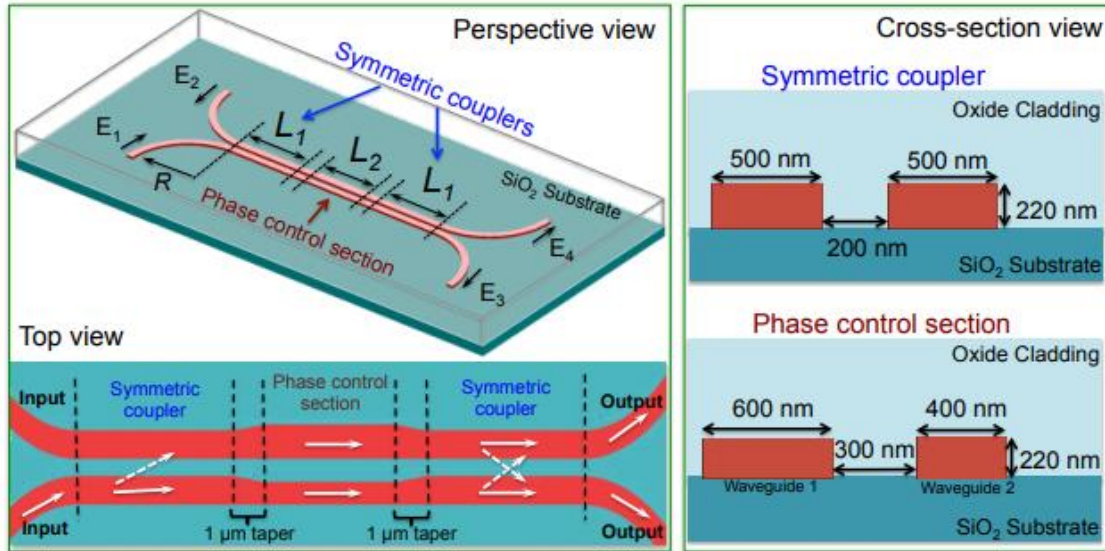


Fig. 12. Schematic of broadband directional coupler [37].

Some other complex designs have been developed to work as polarization beam splitters (PBS) with asymmetrical bent directional couplers [38], as it is shown in Fig. 13. For ultra-short polarization beam splitters, some researchers report that an optimized asymmetrical coupling system is a better approach than symmetric directional couplers. This design flexibility gives the designer the option to modify the waveguide dimensions to satisfy the phase matching condition for only one polarization.

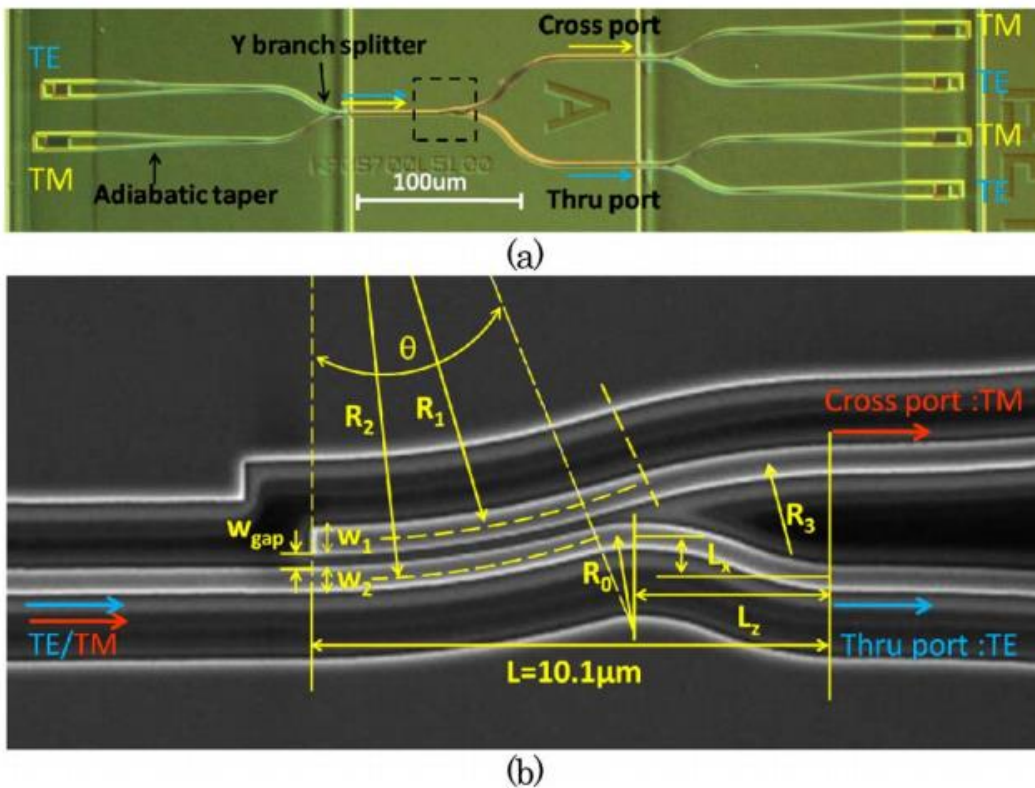


Fig. 13. Silicon polarization beam splitter with an asymmetrical bent directional coupler. [38]  
(a) Image of the fabricated polarization beam splitter. (b) SEM picture for the bent directional coupler.

### 1.4.3 Directional couplers combining more than one material

One step further is the addition of additional materials, such as phase change materials, on the top of the waveguides. In Fig. 14 there is an example of a non-volatile photonic switching using an asymmetric silicon nitride directional coupler and a phase change material (in this case,  $\text{Ge}_2\text{Sb}_2\text{Se}_4\text{Te}_1$ ) [39]. By using this type of configuration, it is possible to switch between both branches by modifying the state of the material on top (from/to amorphous and crystalline, the two states of the chalcogenide). Therefore, depending on the desired performance, the signal will couple to the other waveguide or not.

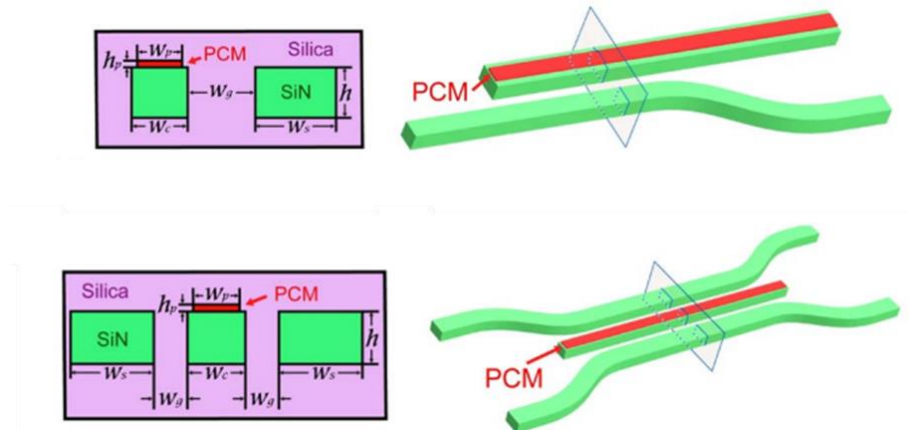


Fig. 14. Two configurations of broadband non-volatile photonic switches based on optical phase change materials. 1x2 switch at the top image. 2x2 switch at the bottom image [39]

A different concept is depicted in Fig. 15. In this device there is a directional coupler in which the waveguides are made with different materials (silicon and silicon nitride) [40]. This recent study shows the possibility of coupling two different materials in a directional coupler, which is the aim of the work proposed in this thesis. However, the combination with phase change materials shown in previous figures, together with an asymmetric dual material directional coupler, has not been reported yet.

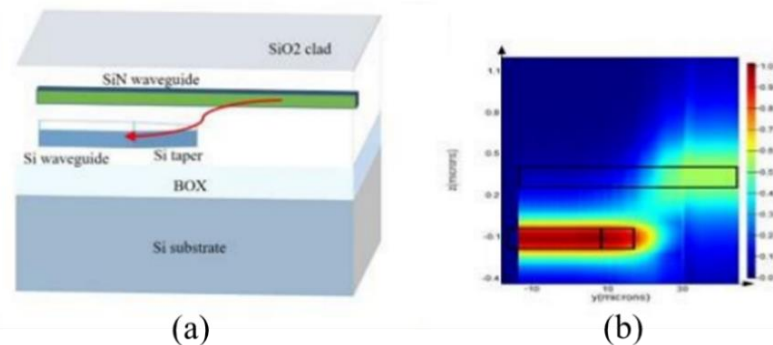


Fig. 15. Si-SiN dual-layer directional coupler. [40]. (a) Schematic of the directional coupler. (b) Light intensity transfer between two layers.

## Chapter 2. Objectives, motivation and methodology

### 2.1 Objectives

The main objective of this work is to design an asymmetric directional coupler combining silicon and silicon nitride. The device will be used to feed a hybrid GST/Si waveguide and improve the performance of the non-volatile switching functionality provided by GST. In particular, the matching condition between the Si and SiN waveguides is analysed in depth.

The following specific objectives have been set to accomplish the mentioned above:

- Review of reported asymmetric directional couplers and hybrid structures.
- Modal analysis of silicon and silicon nitride by using straight waveguides.
- Optimization of the phase matching condition for different Si-SiN combinations.
- Design of the asymmetric Si-SiN directional coupler.
- Final discussion about the obtained results and proposal of future work.

### 2.2 Description and motivation of the device to be designed

The configuration proposed in this work is depicted in Fig. 16. This asymmetric directional coupler, which is optimized a wavelength of 1550 nm, uses the silicon waveguide to transmit the data, meanwhile the silicon nitride waveguide is the control signal for driving the switching. The reason is that SiN waveguides permit the injection of high-power optical signals without affecting the two-photon absorption (TPA) existing in silicon. Nevertheless, the opposite configuration (using the SiN as data signal and Si as control signal) is analysed as well because it could be interesting to perform bi-directional coupling if needed.

On the other hand, there is a layer of a phase change material on top of the silicon waveguide at the output. Si/GST technology and its all-optical switching capabilities can be exploited in this configuration, combining routing and switching at the same time. However, GST is not the only possibility. Vanadium dioxide ( $\text{VO}_2$ ) could be used for similar purposes, taking advantage of its potentially faster switching times.

Notice that all the structures are surrounded by a silicon dioxide cladding (dark blue in Fig. 17). The function of this material is protecting the structures from dust or oxidation.

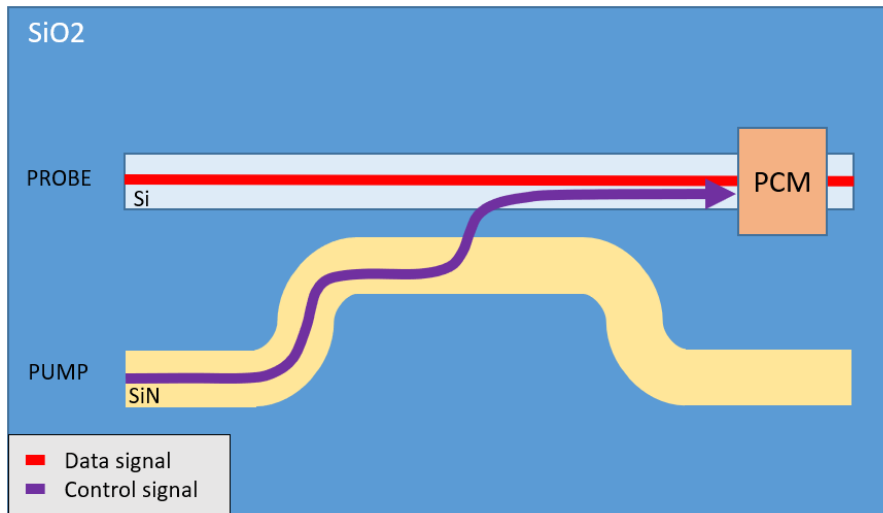


**Fig. 16. Top-view schematic of the proposed asymmetric Si-SiN directional coupler + phase change materials.**

Fig. 17 shows the transversal section of the directional coupler in the coupling region. The silicon waveguide follows the standard dimensions (220-nm-height, 500-nm-wide) and, therefore, the parameters that can be modified to achieve the phase matching condition are the gap between waveguides and the dimensions of the silicon nitride structure. Nevertheless, some other silicon widths will also be tested, as it will be explained in the sections below. On the other hand, the minimum gap between waveguides will be fixed by fabrication constraints to a value of 100 nm.

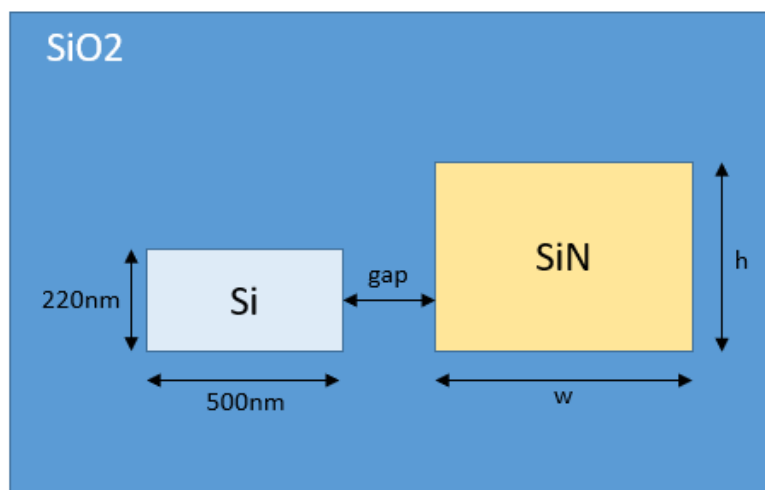


**Fig. 17. Transversal section of the Si-SiN coupling region.**

As it was previously mentioned, directional couplers are widely used for multiple applications in photonics. However, there are several differences from the simplest configurations presented in the introduction and the structure shown in Fig. 16 and Fig. 17. The combination, at the same time, of an asymmetric directional coupler made of two materials (Si-SiN) and a phase change material at the output enables the performance of some of the functionalities shown in the examples of the introduction, reducing the footprint of the devices.

### 2.3 Methodology and design tools

In order to fulfil the objectives mentioned above, the methodology presented in Fig. 18 has been followed. Starting from a deep documentation period, getting familiar with the current technologies and configurations of directional couplers, some preliminary simulations of simple photonic structures were carried out in order to learn the software needed. After this familiarization with the design tools, the next steps were simulating the mode profiles of the waveguides made of silicon and silicon nitride. Then, the gross of the work was related to finding the best phase matching condition of the asymmetric directional coupler, including numerous parametric simulations. With the different phase matching conditions obtained, various directional couplers were simulated and analysed with a propagation method software. Therefore, this work is mainly composed of documentation, simulation and analysis of results, involving a huge workload in terms of analysis and processing the data obtained.

This work was carried out in the Nanophotonics Technology Center (NTC) of Valencia, and it was supervised by Prof. Pablo Sanchis Kilders<sup>1</sup> and PhD candidate Jorge Parra Gómez.

The software programs employed to make the simulations are integrated in the RSoft CAD Environment of Synopsis<sup>2</sup>. For the analysis of the modal profile of the structures, the program used is FemSIM, which is a mode solver based on Finite Element Method (FEM). Moreover, the directional coupler was simulated with the propagation method software BeamPROP, which is based on an advanced finite-difference from Synopsis. Finally, the last program used from the RSoft environment is FullWAVE, which is based on Finite-Difference Time-Domain (FDTD) method. On the other hand, MATLAB was the software chosen to process the data and plot the information of the phase matching coincidences.

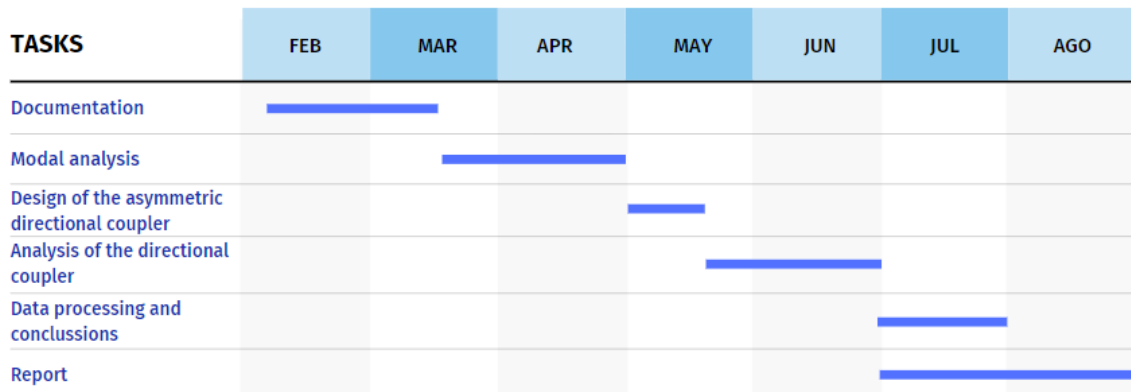


Fig. 18. Time diagram of the tasks carried out in this thesis.

<sup>1</sup> Head of Photonics Integrated Devices research line. <http://orcid.org/0000-0003-2984-4218>

<sup>2</sup> <https://www.synopsys.com/photonic-solutions/rsoft-photonic-device-tools/cad-environment.html>

### Chapter 3. Modal analysis of the waveguides of the directional coupler

The first step in the design of the directional coupler is the analysis of the guided modes both in the silicon waveguide and the silicon nitride waveguide. For this purpose, the program employed is FemSIM, which requires the introduction of the material parameters involved (i.e., refractive index). The software already has a set of pre-loaded values for the materials employed. However, the refractive indices used were chosen from the information obtained in previous results in the NTC, and they are listed in Table 3.

Material	Refractive index
Silicon dioxide (SiO <sub>2</sub> )	1.444
Silicon (Si)	3.476
Silicon nitride (Si <sub>3</sub> N <sub>4</sub> )	1.990
GST (Ge <sub>2</sub> Sb <sub>2</sub> Te <sub>5</sub> ) - Amorphous	3.798 + 0.074j
GST (Ge <sub>2</sub> Sb <sub>2</sub> Te <sub>5</sub> ) - Crystalline	6.462 + 1.074j

Table 3. Refractive indices of the materials of the directional coupler.

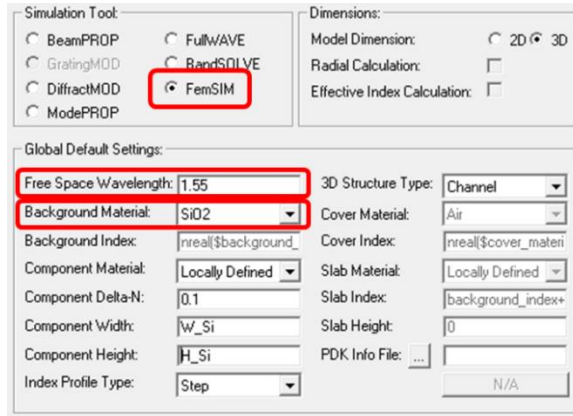
The guiding mechanism of the waveguides employed is based on total internal refraction (TIR). It is desired to use single-mode waveguides in order to avoid coupling of high-order modes that could perturbate the performance of the directional coupler. This fact determines the maximum size of the structures. On the other hand, the minimum sizes are limited by the diffraction limit, which says that the light in rectangular waveguides cannot be longer confined in the core if the size is reduced below a certain point. This value can be estimated by using the equation (3).

$$w < \frac{\lambda}{2n_1} \quad (3)$$

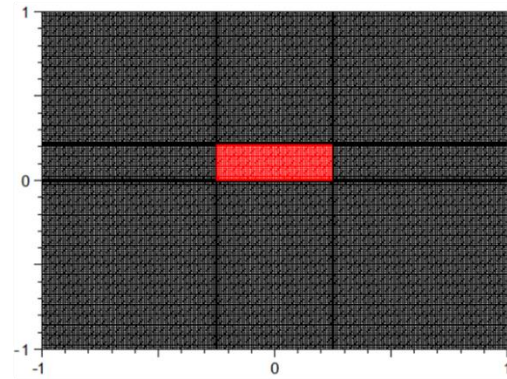
where  $n_1$  is the refractive index of the core in the rectangular waveguide.

#### 3.1 Modal analysis of the silicon waveguide

Starting with the silicon waveguide, the simulated structure follows the standard dimensions presented in Fig. 17 (i.e., the width is 500 nm, and the height is 220 nm). By using these parameters, a straight silicon waveguide was created in the RSoft software. Afterwards, the simulation window must be configured, as described in Fig. 19(a). Then, the mesh must be defined to guarantee the precision in the results. FemSIM permits the creation of nonuniform meshes, which enables defining different mesh sizes depending on the area. As it is shown in Fig. 19(b), it is possible to create meshes that are more accurate on the edges of the structures, while the rest working area has a bigger step size, reducing the computation load. Finally, the last values to introduce in the software are the number of modes to compute and the maximum number of iterations.



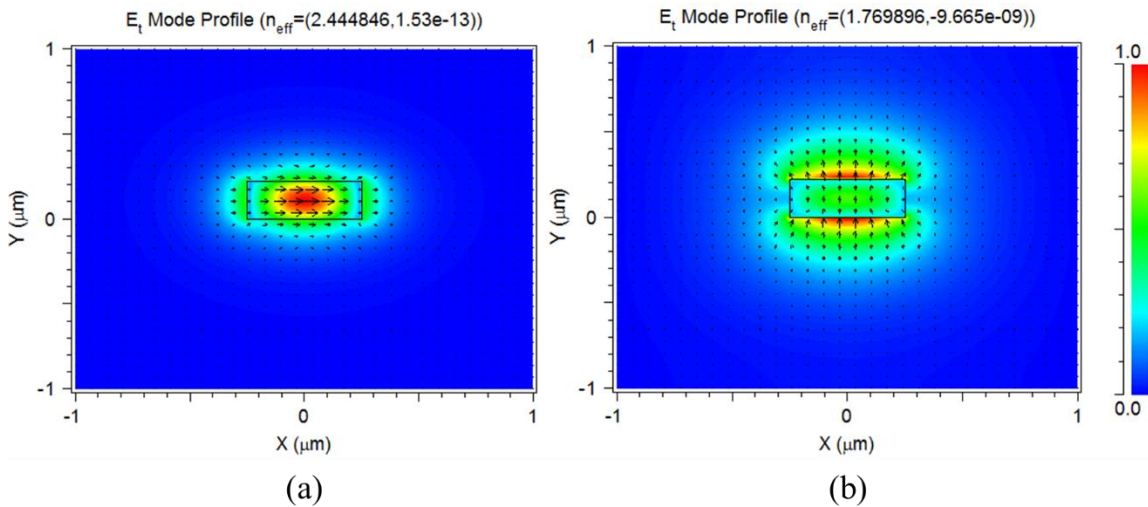
(a)



(b)

Fig. 19. (a) Settings of the FemSIM simulation of the silicon waveguide. (b) Nonuniform mesh for the simulation of the silicon waveguide.

After running the simulation, the two fundamental modes (TE and TM) at 1550 nm are obtained. On the left (Fig. 20(a)) it is shown the electric field of the TE mode, while the right plot (Fig. 20(b)) corresponds with the electric field of the fundamental TM mode.



(a)

(b)

Fig. 20. Mode profile of the fundamental modes of the silicon waveguide obtained with FemSIM. (a) TE mode. (b) TM mode.

The values required for designing the directional coupler are the effective indices shown at the top of the previous plots ( $n_{eff}$ ). The reason is that the aim is to achieve the maximum power coupled from one waveguide to the other, and that fact happens when the phase matching condition is obtained (i.e., the effective index of the silicon waveguide is equal to the silicon nitride waveguide index). Table 4 collects the indices mentioned above, both in TE and TM polarizations.

Standard silicon waveguide (h = 220 nm, w = 500 nm)	
Mode	$n_{eff}$
TE	2.444846392
TM	1.769895554

Table 4. Effective index of a standard silicon waveguide computed with FemSIM.

### 3.2 Modal analysis of the silicon nitride waveguide

The dimensions of the silicon nitride waveguide are one of the design parameters to optimize. Following the same criteria of the silicon waveguide, the single-mode performance is preferred to avoid coupling of high-order modes. However, due to the difference in the refractive indices of the Si and SiN, the dimensions of the silicon nitride waveguide with similar effective index are significantly bigger than the sizes of the standard silicon waveguide. This means that some high-order modes could appear in the silicon nitride structure, and they will affect the behaviour of the directional coupler. It should be taken into account when analysing the results of the final device.

RSoft contains a simulation tool which permits parametric sweeps of any variable used in the designs. It is called Multi-Variable Optimization and Scanning Tool (MOST)<sup>3</sup> and consists of a wizard where user fixes the values of the parameters to make the sweep and the number of steps, depending on the precision required. The sizes were chosen after a preliminary test by considering a 500-nm-high and 1200-nm-wide SiN waveguide, as depicted in Fig. 21. Observing the effective index at the top of each plot it is obvious that the dimensions of the structure must be bigger. The reason is that in a standard silicon waveguide, the  $n_{eff}$  in TE is higher than the refractive index of the SiN. Therefore, the condition  $n_{eff} > n_{core}$  cannot be met and the effective index will be always lower than the value of the silicon waveguide (see Fig. 21(a)). On the other hand, for TM polarization (Fig. 21(b)) the effective index reported is 1.643944 (versus the 1.769895 of the silicon waveguide). Thus, the directional coupler will be designed taking into account this polarization in the silicon waveguide.

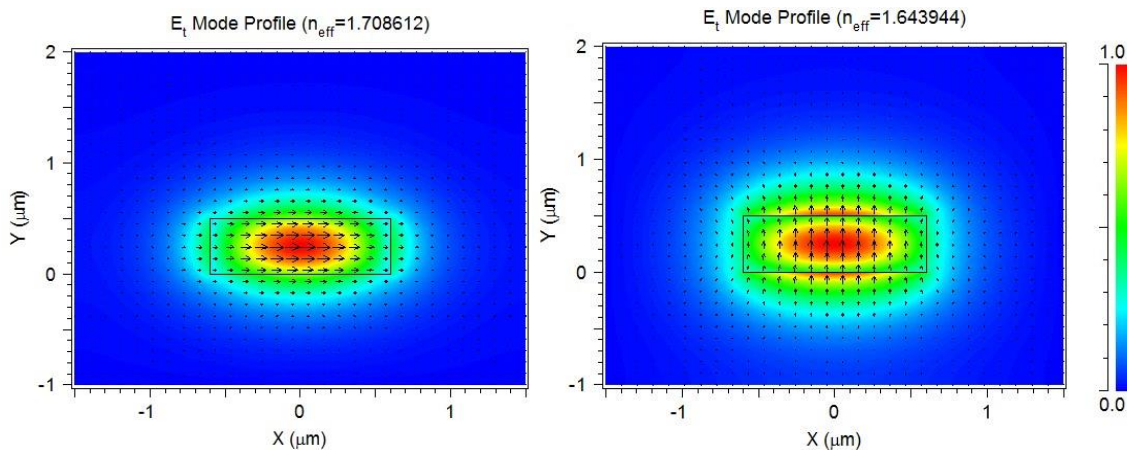


Fig. 21. Mode profile computed with FemSIM of the fundamental modes for a 500-nm-high and 1200-nm-wide silicon nitride waveguide. (a) TE mode. (b) TM mode.

<sup>3</sup> <https://www.synopsys.com/photonic-solutions/rsoft-photonic-device-tools/most.html>

Fig. 22 shows the MOST window with the values employed for the parametric simulation. Considering the preliminary simulation of the SiN waveguide, they are on the range of the possible values of phase matching. Therefore, the last step is running the parametric sweep. For this purpose, the same simulation window shown in Fig. 19(a) is used, obtaining a set of results combining the width and the height entered. The wavelength was fixed to 1550 nm.

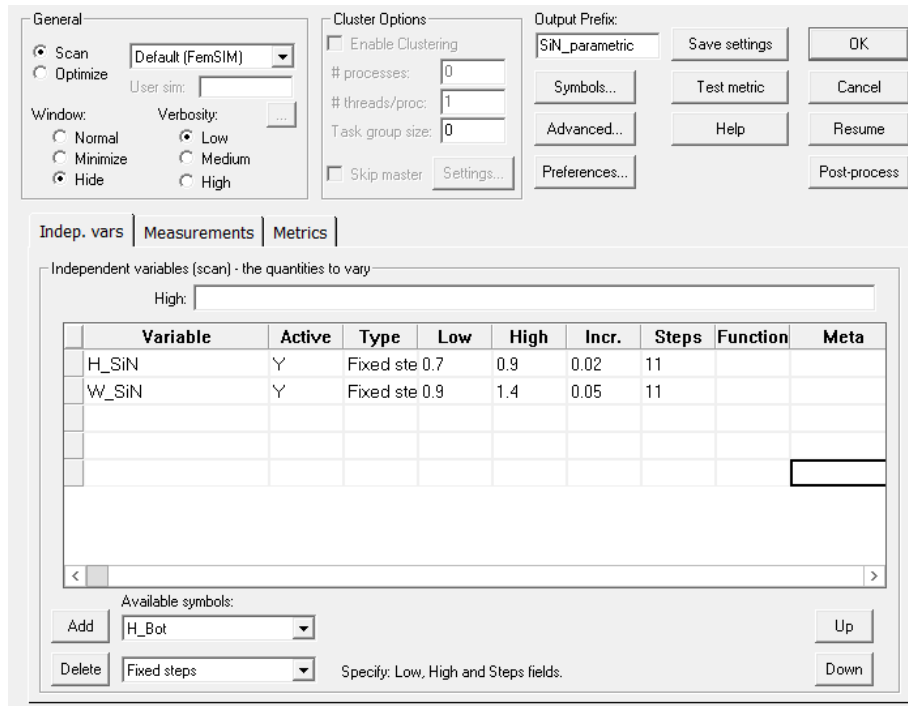


Fig. 22. Settings of the MOST simulation tool for the sweep of the silicon nitride waveguide sizes.

There are 121 combinations of widths and heights for the silicon nitride waveguide using the values shown in the MOST wizard. Apart from the plots shown before, FemSIM generates ASCII files with the effective indices of the simulations. Therefore, there is the possibility of processing the data using an external program instead of checking the coincidences one by one.

MATLAB is the software employed for this purpose. After loading the ASCII files, the program created compares the values of the 121 effective indices in TE and TM polarization, as it is shown in the graph of Fig. 23. The red line represents the effective index of the silicon waveguide surrounded by silica for TM polarization, because the TE value is out of the ranges reported by simulation. At the top of the figure, the coincidences between the effective index of the Si waveguide in TM and the effective indices of the SiN waveguide in TE are indicated. This is not the aim of this work, because changing the polarization of the signal is usually not possible unless the waveguide configuration is changed (e.g., placing a metal surface on top of the waveguide). Nevertheless, due to the proximity of the phase matching values of both polarizations, it should be considered because it may affect on the supermodes generated in the directional coupler.

On the other hand, the coincidences in TM polarization are highlighted at the bottom of the Fig. 23. Considering the plot, up to nine values could be used to create the straight section of the directional coupler. All of them are collected in Table 5, showing the correspondent dimensions of the silicon nitride waveguides.

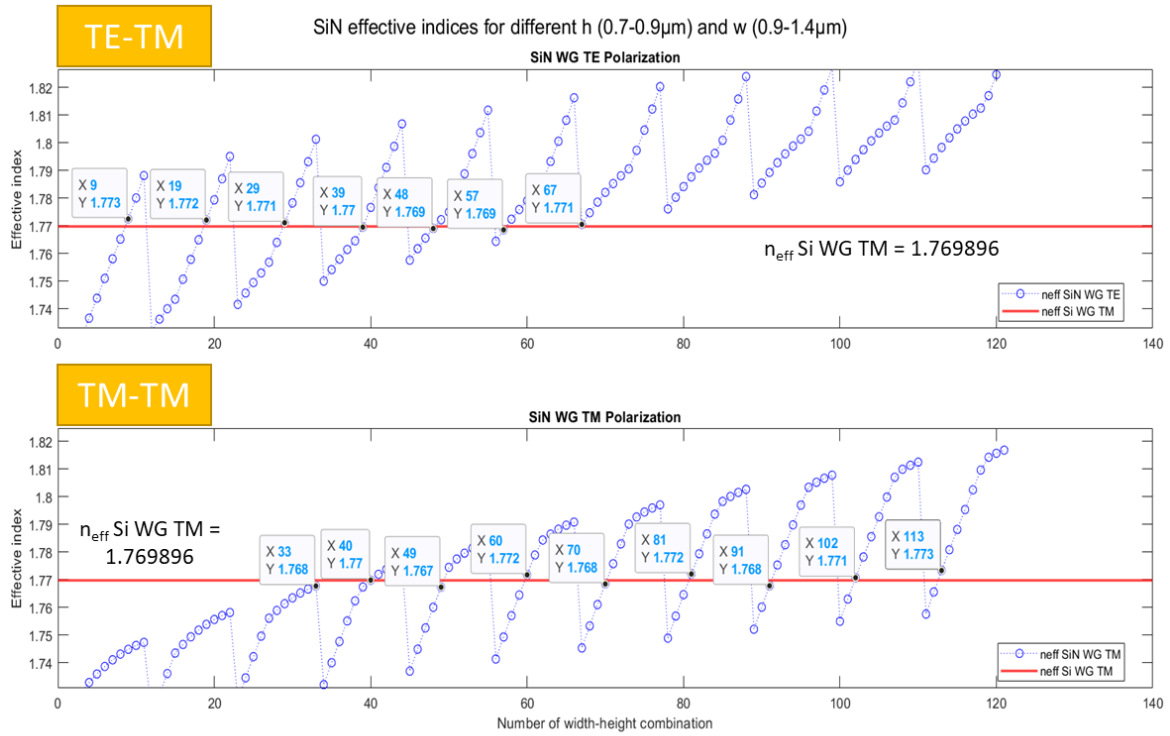


Fig. 23. Results of the MOST simulation of the SiN waveguide in TE and TM polarizations.

Effective index coincidences SiN-Si (TM polarization)		
Identifier	SiN dimensions (width x height)	$n_{eff}$
1	0.90 x 1.00 $\mu\text{m}$	1.767754197
2	0.82 x 1.05 $\mu\text{m}$	1.769868731
3	0.78 x 1.10 $\mu\text{m}$	1.767334223
4	0.78 x 1.15 $\mu\text{m}$	1.771786809
5	0.76 x 1.20 $\mu\text{m}$	1.768494606
6	0.76 x 1.25 $\mu\text{m}$	1.772099137
7	0.74 x 1.30 $\mu\text{m}$	1.767842650
8	0.74 x 1.35 $\mu\text{m}$	1.770745397
9	0.74 x 1.40 $\mu\text{m}$	1.773339987

Table 5. Effective index coincidences between the Si and SiN waveguides for TM polarization.

## Chapter 4. Design of the asymmetric directional coupler

### 4.1 Design parameters. Influence on the performance and limitations.

#### 4.1.1 Influence of the design parameters

The influence of the dimensions of the silicon and silicon nitride waveguides is clear, because the phase matching condition will be met for only a group of widths-heights. Despite this, there are some reasons to decide which is better. From the point of view of footprint, the more asymmetric is the directional coupler, the more differences appear in relation to a symmetric design. Therefore, due to the fixed dimensions of the silicon waveguide, it would be interesting to employ similar width or height in the silicon nitride waveguide. For this reason, it is preferred to use lower heights among the possible combinations showed in the previous section. Moreover, width and height proportions should be similar in both waveguides. By dividing the height and the width of the silicon waveguide, an aspect ratio of 2.27:1 (500 nm x 220 nm) is obtained. It would be desirable using ratios in the same order of magnitude for the SiN structure.

On the other hand, depending on the used gap, the field vectors of the coupled signal can be rotated. From the point of view of coupled power, the closer the waveguides, the more power transmitted from one to the other. Therefore, the best solution should be using the closest gap available (fixed by fabrication constraints). However, if the waveguides are too close, the resulting supermodes are not as expected, thus there is a trade-off between maximum power and the best quality of the signal obtained (i.e., maintaining the characteristics of the TM mode signal).

#### 4.1.2 Limitations

Firstly, in terms of phase matching, the limitations are obvious. It is not possible to place waveguides of similar sizes of silicon and silicon nitride to create a directional coupler. This fact can be a problem in terms of fabrication because it may require extra lithography steps.

Secondly, due to the size of the SiN structure, it is not possible to totally avoid high-order modes, thus they could affect on the supermodes generated in the coupler.

Finally, the bi-directional coupling could not be achieved due to the high differences in terms of size. Therefore, the silicon waveguide will not transfer the power to the silicon nitride structure.

## 4.2 Analysis of the configurations available

#### 4.2.1 Supermodes

The nine coincidences in TM polarization listed in Table 5 will be simulated in this section. For all of them, the gap between waveguides is 150 nm because it is a distance high enough to avoid problems in fabrication but close enough to achieve a good coupling between structures.

In order to distinguish the dimensions used on each simulation, an identifier has been assigned to every combination of width-height, as shown in Table 5. Using the first combination (i.e., a silicon standard waveguide and a 0.90 x 1.00  $\mu\text{m}$  SiN waveguide), the results of the supermodes obtained are shown in Fig. 24 and Fig. 25.

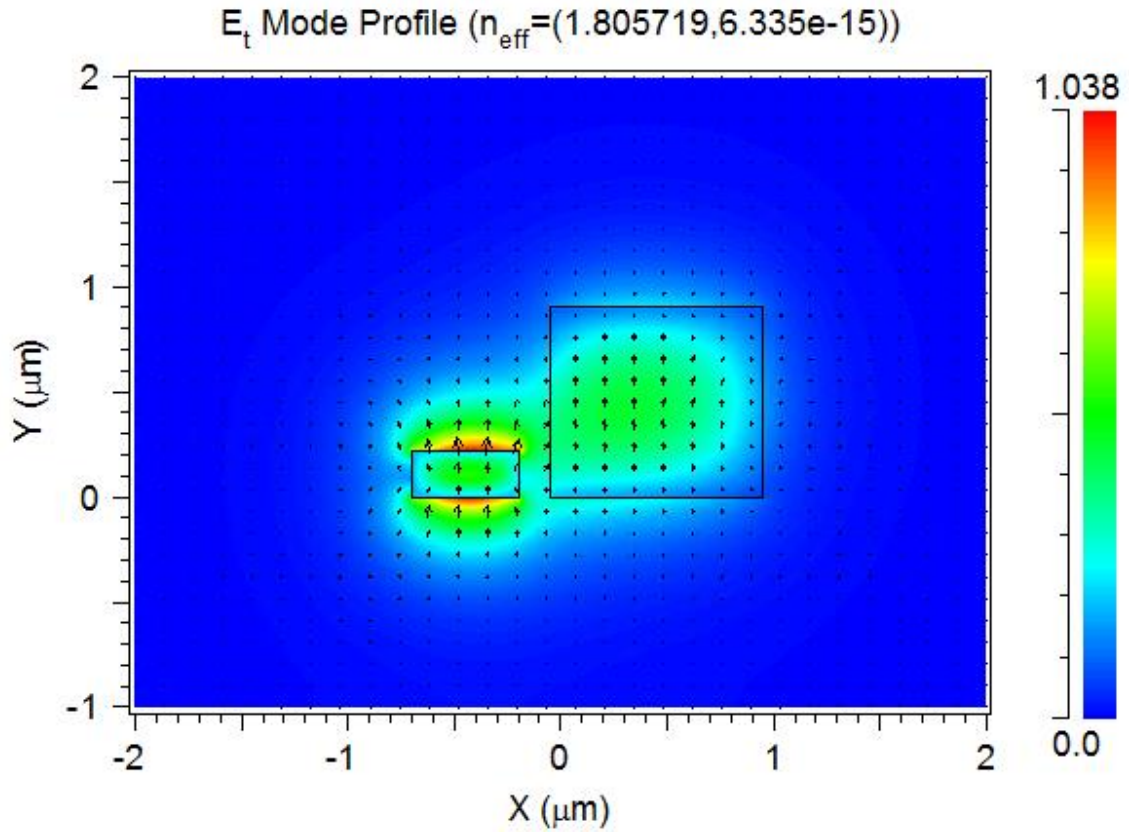


Fig. 24. Even mode of the directional coupler with the identifier #1.

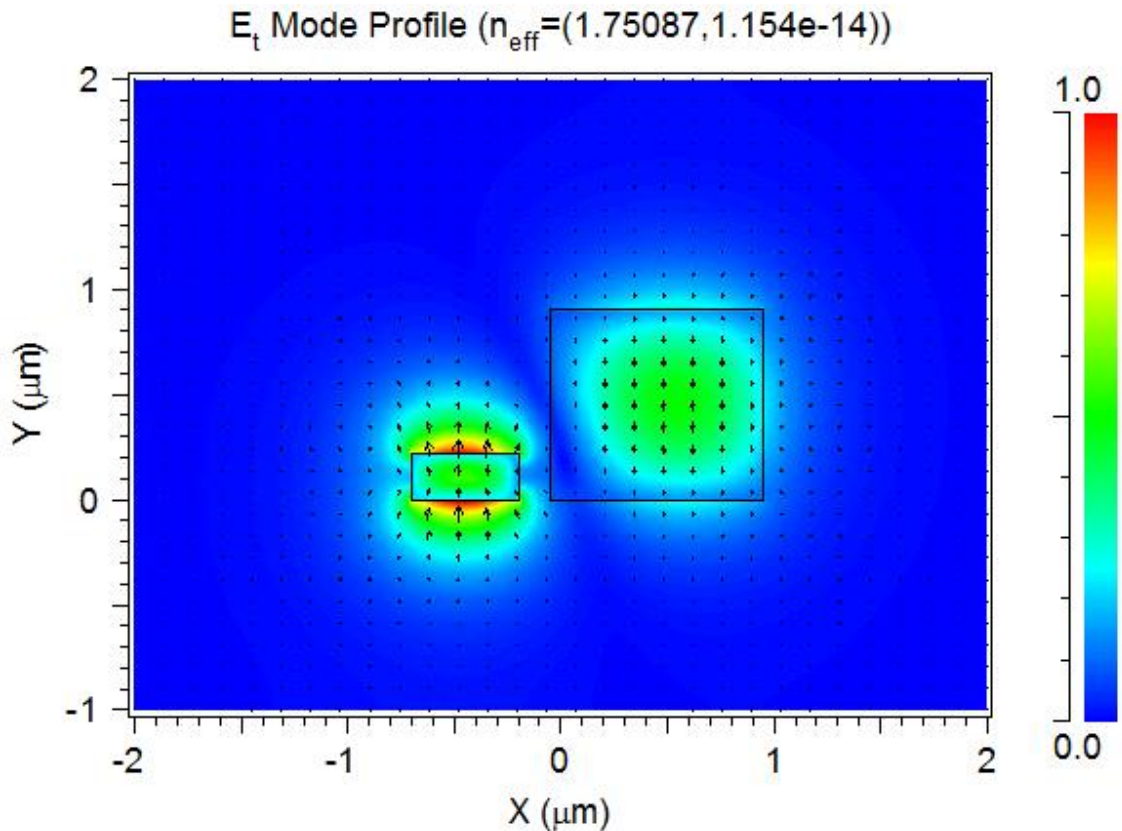


Fig. 25. Odd mode of the directional coupler with the identifier #1.

Both supermodes can be recognized by looking at the direction of the electric fields (represented by the arrows). In Fig. 24 the electric fields through both waveguides have the same direction, thus it is the even mode, whereas in Fig. 25 the arrows are in the opposite direction, which means that it is the odd mode.

It is remarkable that the strength of the electric fields is not equal in both waveguides, as it occurs in the traditional symmetric directional coupler, as explained in the introduction. This is one of the limitations expected for this kind of coupling structure, which indicates that it will not be able to transfer all the power from one branch of the coupler to the other. Therefore, the aim of this design is obtaining the best performance among the results obtained. Results of the other potential structures are shown in Fig. 26 and Fig. 27, where the left columns are the even modes and the right columns represent the odd modes.

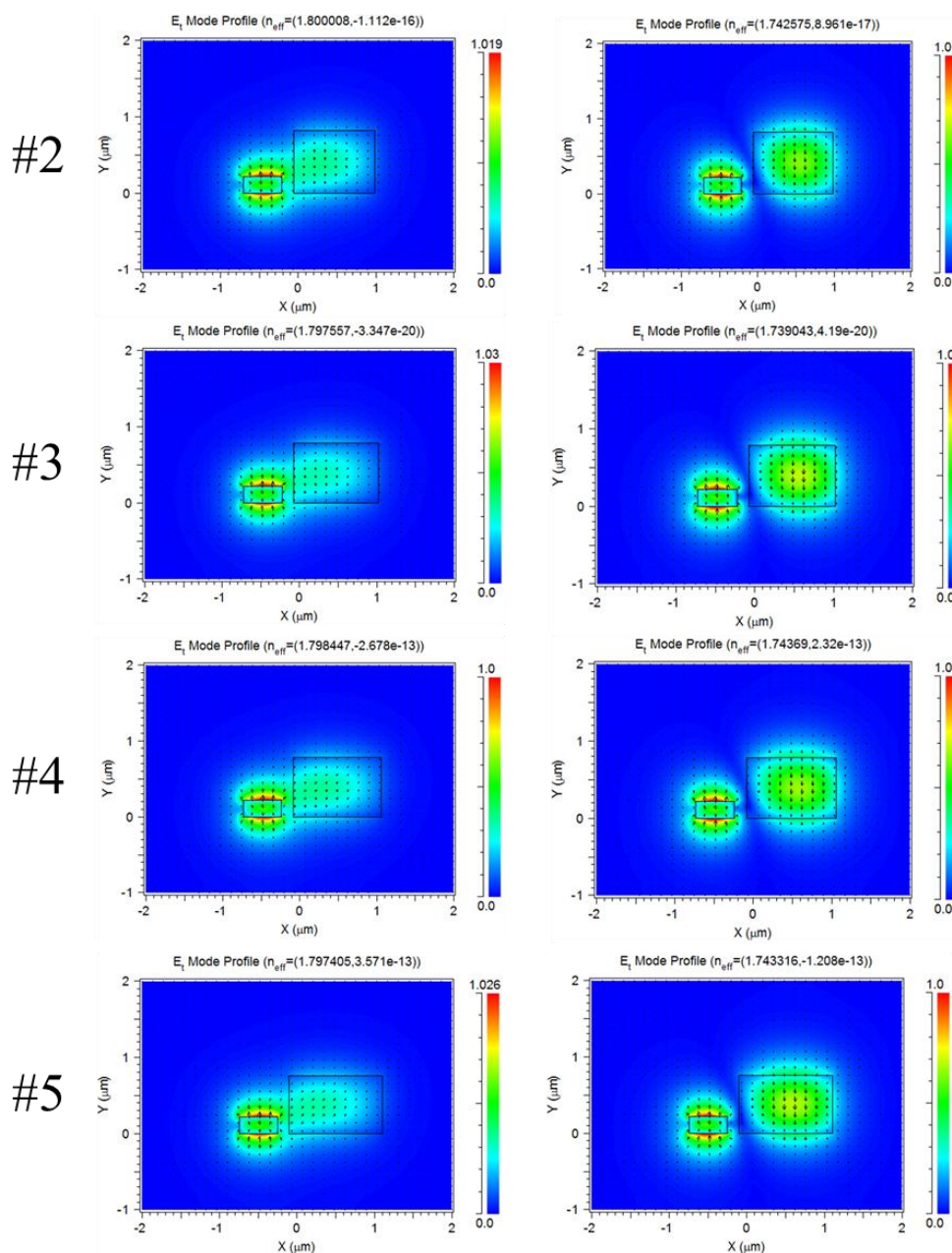


Fig. 26. Even mode (left) and odd mode (right) for the couplers with identifiers 2, 3, 4 and 5.

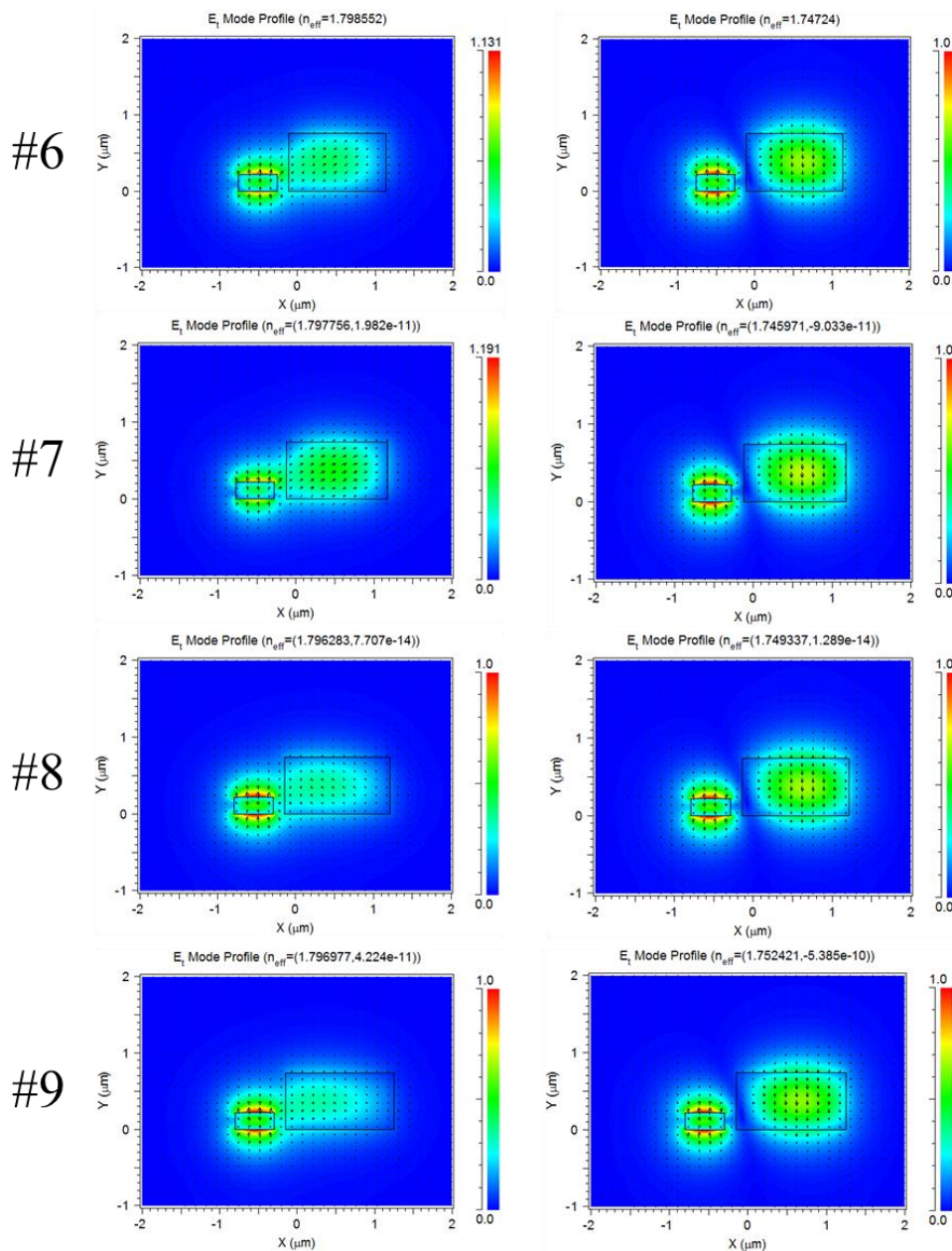


Fig. 27. Even mode (left) and odd mode (right) for the couplers with identifiers 6, 7, 8 and 9.

All the supermodes shown in the previous figures are quite similar. In the odd mode (right column) the differences between the results are not easy to appreciate and, therefore, the decision of which is the best is not obvious. However, focusing on the left column it is easier to view the changes in terms of power coupled by observing the intensity of the electric fields. By using the colour scale depicted on the right of each plot it is possible to see that, for example, the fields are stronger in the coupler number 7 than the structure 8. These results will be analysed when comparing the power coupled in the BeamPROP simulations that will be carried out in next sections.

On the other hand, by using the effective indices shown at the top of each plot, the beat length ( $L_B$ ) of each directional coupler is computed using the expression presented in equation (1). The  $L_B$  parameter represents the length needed for the optical power to transfer completely from one waveguide to another in the directional coupler. Thus, it must be taken into account when simulating the structure with BeamPROP.

Effective index coincidences SiN-Si (TM polarization)			
Identifier	$n_{eff-e}$	$n_{eff-o}$	$L_B$ ( $\mu\text{m}$ )
1	1.805719	1.750870	28.2594031
2	1.800008	1.742575	26.9879686
3	1.797557	1.739043	26.4893872
4	1.798447	1.743690	28.3068831
5	1.797405	1.743316	28.6564736
6	1.798552	1.747240	30.2073589
7	1.797756	1.745971	29.9314473
8	1.796283	1.749337	33.0166574
9	1.796977	1.752421	34.7876829

Table 6. Effective indices of the even and odd mode for the nine structures and its beat length.

#### 4.2.2 BeamPROP simulation

Next step in the design is configuring and performing a simulation of the propagation. For this purpose, the software employed is BeamPROP. By using the values of the beat length computed before, the structures have been configured in the simulator using a length of two times the  $L_B$ .

In order to perform the simulation, it is necessary to indicate the characteristics of the signal injected. A simulation of the modal profile of each waveguide is done by following the same steps done in section 3.2. An example of the signal that will be used in the input port is shown in Fig. 28.

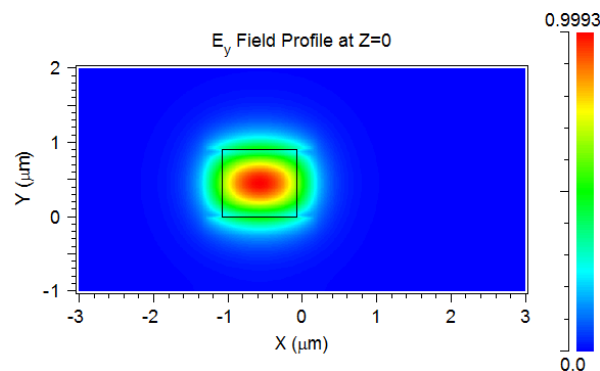
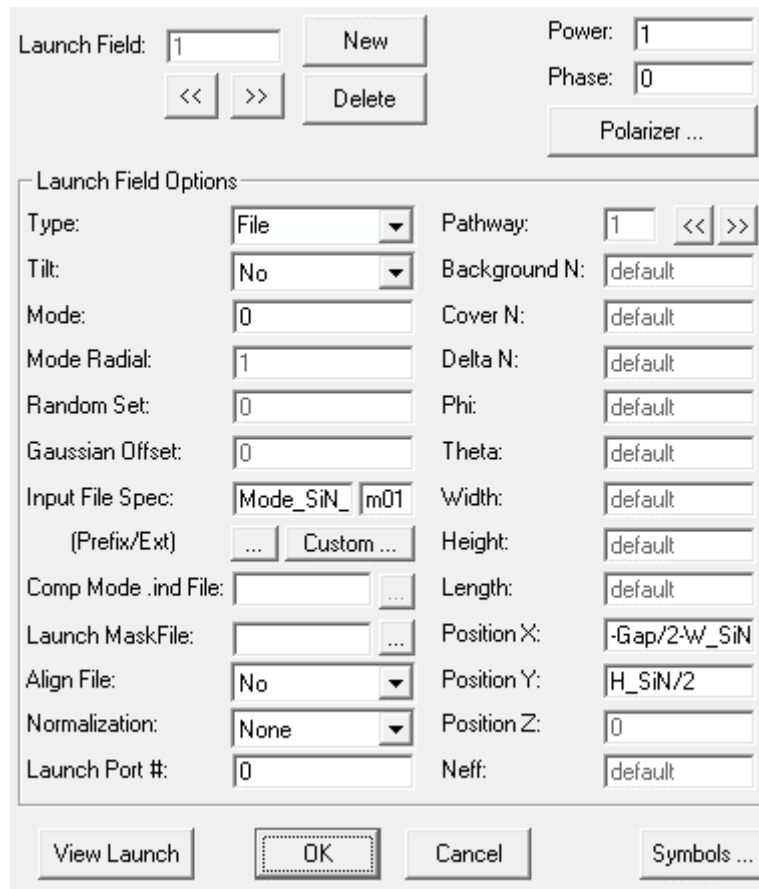


Fig. 28. Example of the input signal injected to the SiN waveguide of the directional coupler.

The window to configure the BPM simulation is shown in Fig. 29. The “launch” is the input port, which has to be chosen as “File”. Then, indicating the appropriate file and the position of the port, the simulation is ready to be run.



**Fig. 29. Settings of the BeamPROP simulation.**

After running the simulation, the obtained results are shown in Fig. 30. Left side (red colour) represents the parallel waveguides, where the signal is injected in the SiN (left). It can be seen that the signal from the silicon nitride waveguide couples partially to the silicon waveguide, describing the periodic response expected. However, looking to the right graphs it is remarkable that the power coupled is about 1/4 of the maximum value (i.e., -6 dB). It can be concluded that the optimal coupling condition is not achieved perfectly. However, considering the huge losses of a silicon waveguide when using high power signals (in Fig. 31, it is remarkable that the insertion loss in silicon waveguides increases drastically after a certain point), the configuration presented here could be still interesting.

The other combinations were also simulated, obtaining similar results to the one shown here. It is important to notice that the structure number 7, which appeared to have stronger coupling between waveguides, reports values about 1/5 of the maximum power (versus the 1/4 shown in Fig. 30)

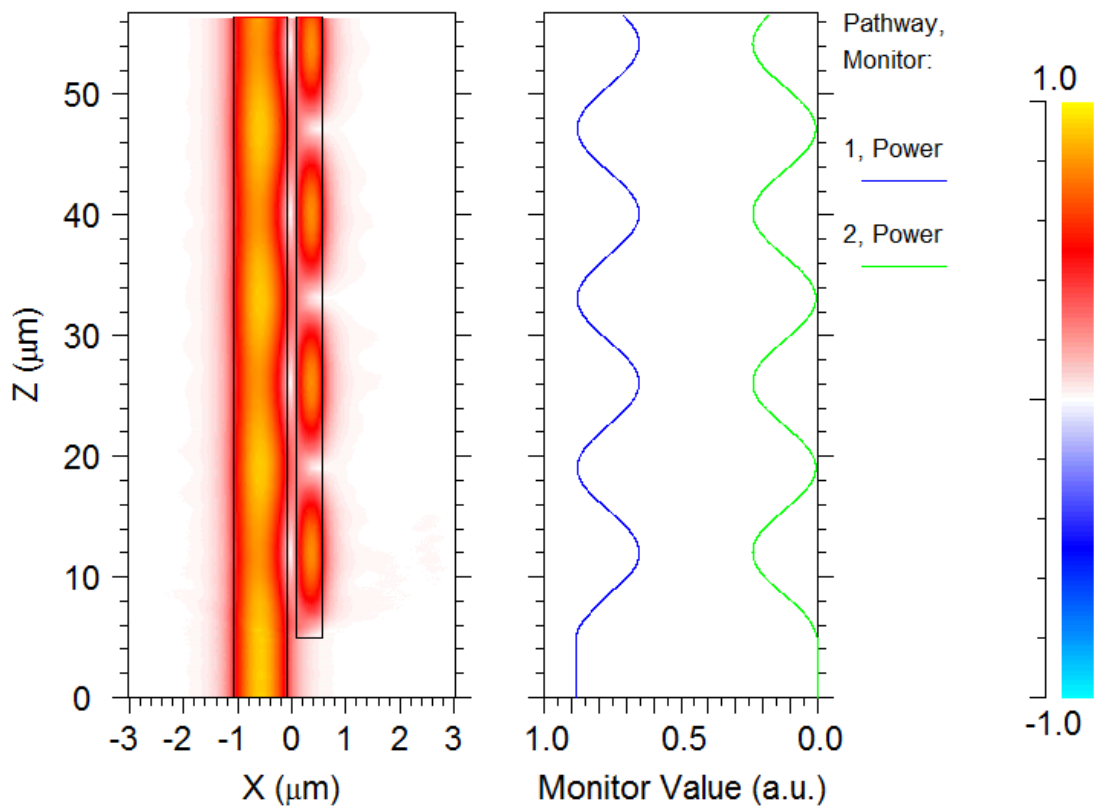


Fig. 30. BeamPROP simulation of the structure with identifier 1.

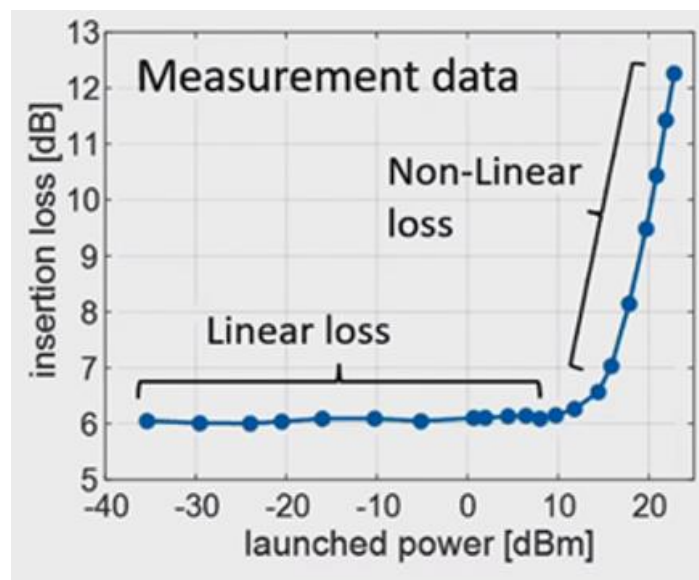


Fig. 31. Insertion loss vs. launched power in C-band for CW light. Two-photon absorption [41].

The problem arising from the use of this bulky structures is that the high-order modes cannot be avoided. Fig. 32 shows two examples of modes generated in the previous structure that may affect the performance. Therefore, in the next section there are some possible solutions to reduce the dimensions of the silicon nitride waveguide.

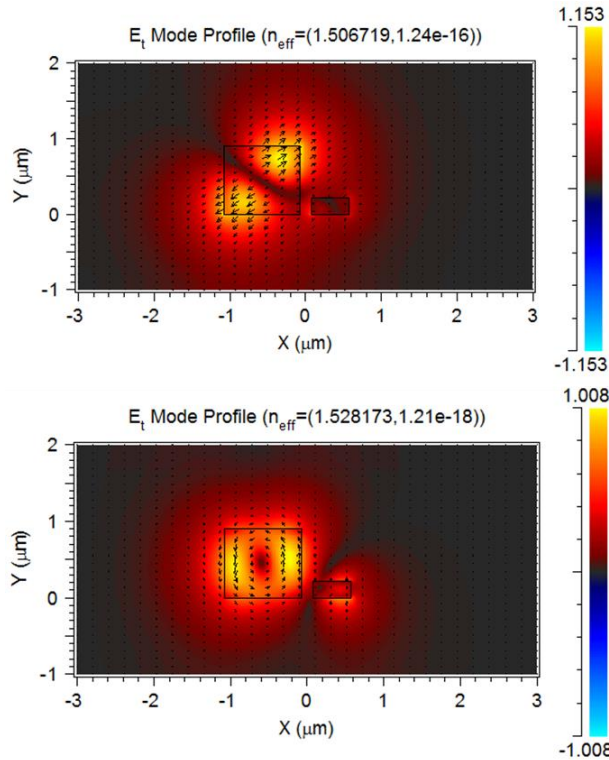


Fig. 32. Two high-order modes of the structure with identifier 1.

#### 4.2.3 Addition of the GST

After the asymmetric directional coupler, the signal injected by the silicon nitride waveguide is guided through the silicon structure. Then, the designed device has a layer of GST which enables the use of the system as a switch. This is possible due to the large change in the effective indices of the GST between its amorphous and crystalline state, as depicted in the next figures. Fig. 33 shows the GST in amorphous for TE and TM polarizations. Then, Fig. 34 represent the analogous simulation but in crystalline state.

By using a 25-nm-thick GST layer, the control signal coupled from the silicon nitride waveguide can change the state of the GST on top with its strong in-plane power [34]. This kind of structure has not been only tested in simulation environments but also in experimental measurements [34]. Therefore, it can be used for the purpose mentioned.

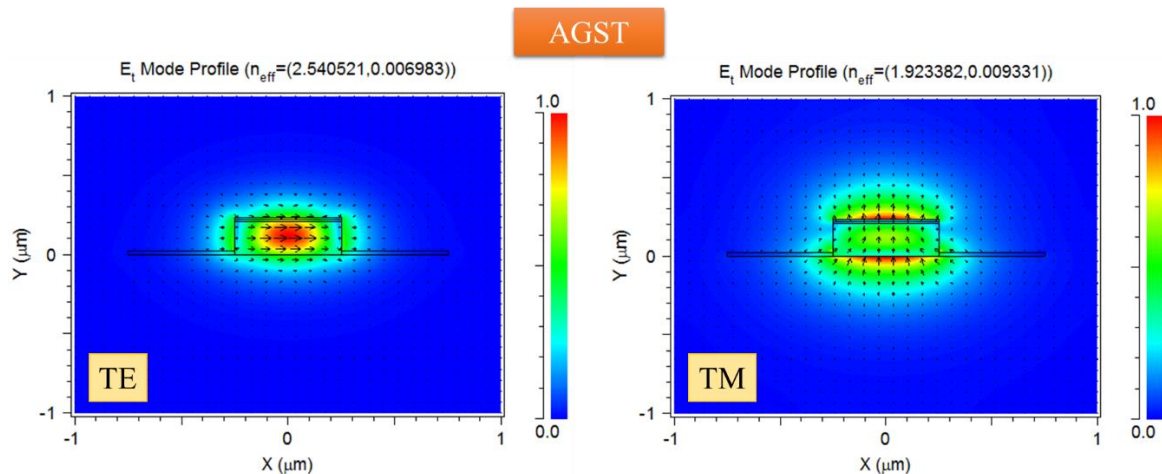


Fig. 33. Simulation of the effective indices of the hybrid Si/GST structure for GST in amorphous state.

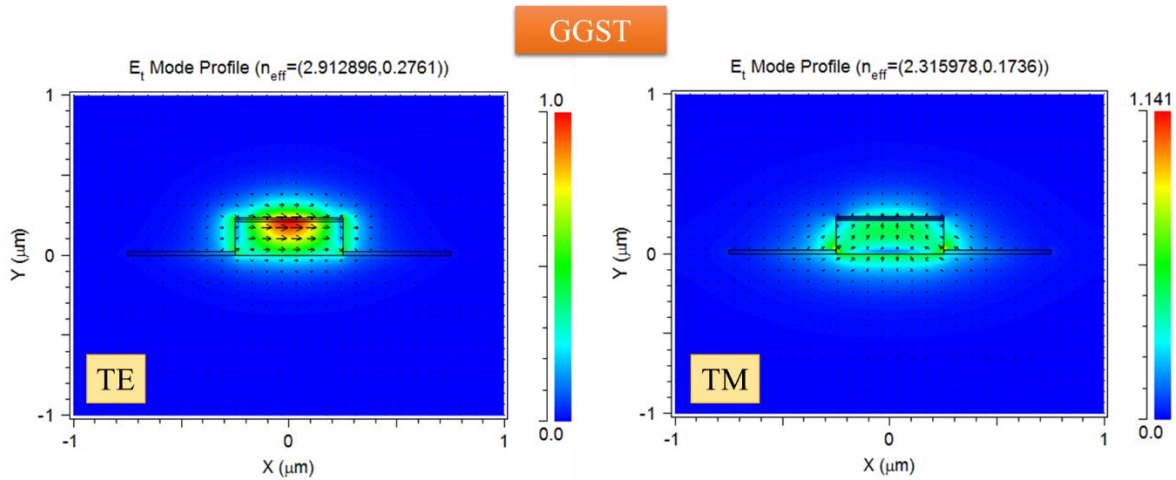


Fig. 34. Simulation of the effective indices of the hybrid Si/GST structure for GST in crystalline state.

### 4.3 Optimal design parameters

The alignment of the two waveguides forming the asymmetrical directional coupler, following the schematic shown in Fig. 35, can improve the performance presented before. The reason is that the electric field vectors in the supermodes are not rotated.

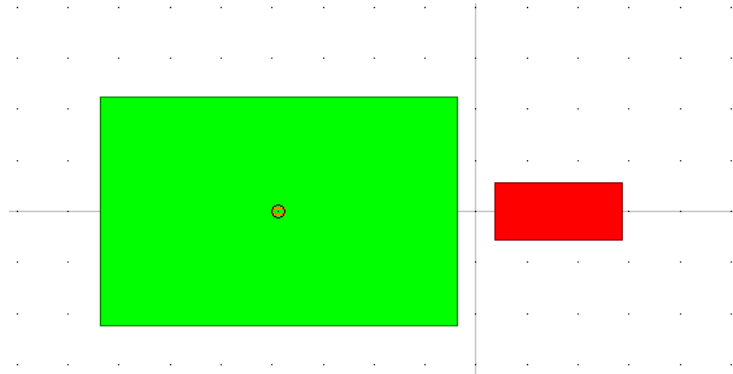


Fig. 35. Cross-section of the structure with identifier 1 changing the alignment of the waveguides.

Fig. 36 shows the BeamPROP simulation of the structure combining the SiN with identifier 1 and the standard silicon waveguide. It is remarkable that the power coupled from the silicon nitride to the silicon waveguide is almost twice the one obtained before. Here, the losses are about 3 dB, whereas with the previous configuration they were about 6 dB and beyond.

Despite the better coupling, this structure could be more problematic in terms of fabrication. If the directional coupler is created in a SiO<sub>2</sub> substrate, the silicon nitride waveguide is partially buried, which is not easy to achieve.

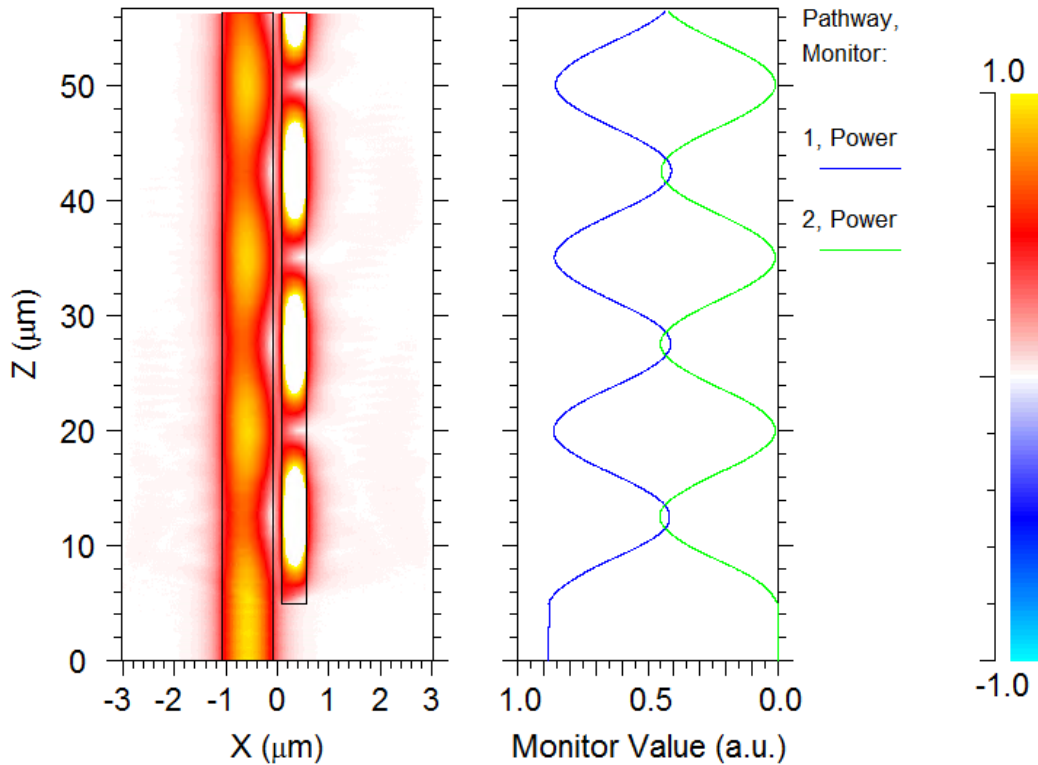


Fig. 36. BeamPROP simulation of the structure with identifier 1 changing the alignment of the waveguides.

#### 4.4 Possible configurations for a new the asymmetric directional coupler

There are some possible configurations that could improve the behaviour of the directional coupler shown above. Firstly, the guiding mechanism of the silicon waveguide could be modified to create smaller structures. For this purpose, one of the configurations analysed was the use of photonic slot waveguides like the one shown in Fig. 37. However, they were discarded because it was not possible to achieve lower effective indices than the ones presented in a standard silicon waveguide.

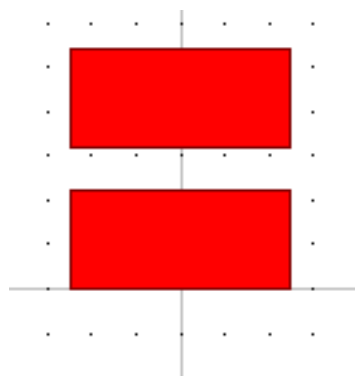


Fig. 37. Cross-section of a silicon slot waveguide.

Another option is changing the dimensions of the silicon waveguide. By reducing the width, the value of the effective index obtained is lower, as depicted in Fig. 38. This means that the cross-section of the directional coupler could also be reduced. Nevertheless, the confinement of the light in the silicon waveguide is not as strong as it is for the standard waveguide.

Si effective indices for a fixed height (220 nm) and different width (100-500 nm)

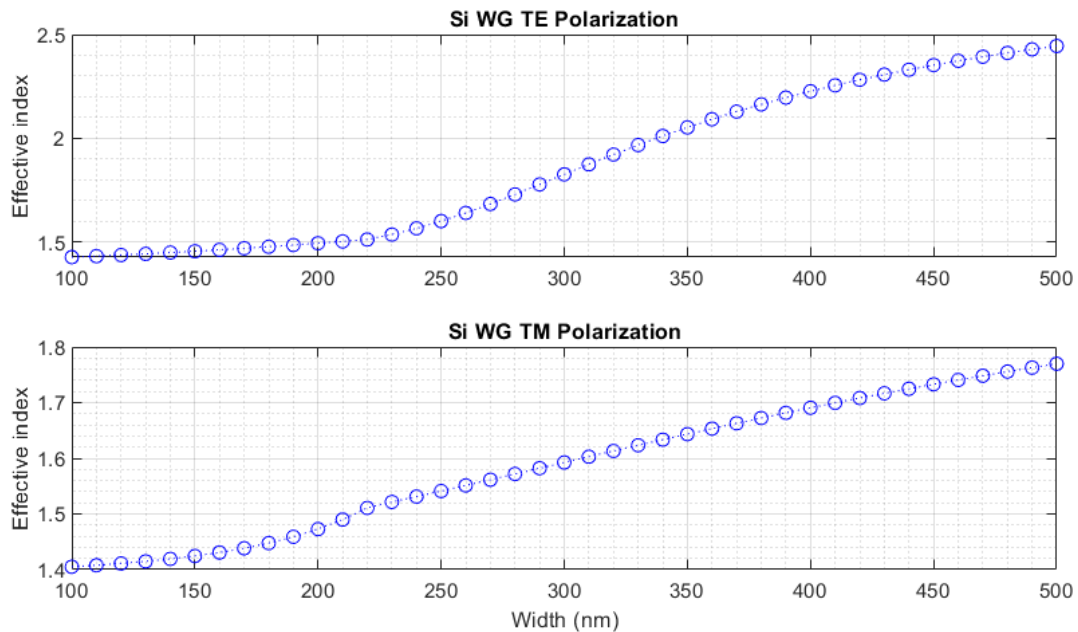


Fig. 38. Effective indices of silicon waveguides with different width.

Finally, one possibility is using sub-wavelength transmission by changing the properties of the silicon waveguide. In order to do that, an analysis of the effective indices for different materials has been done. Sweeping between the refractive index of the  $\text{SiO}_2$  and the value of silicon, the simulation reported the results shown in Fig. 39. The conclusion is that there are several values of equivalent refractive indices (i.e., different materials or a sub-wavelength structure that emulates a material) that could be used.

Effective indices for 220x500 nm WG with different materials

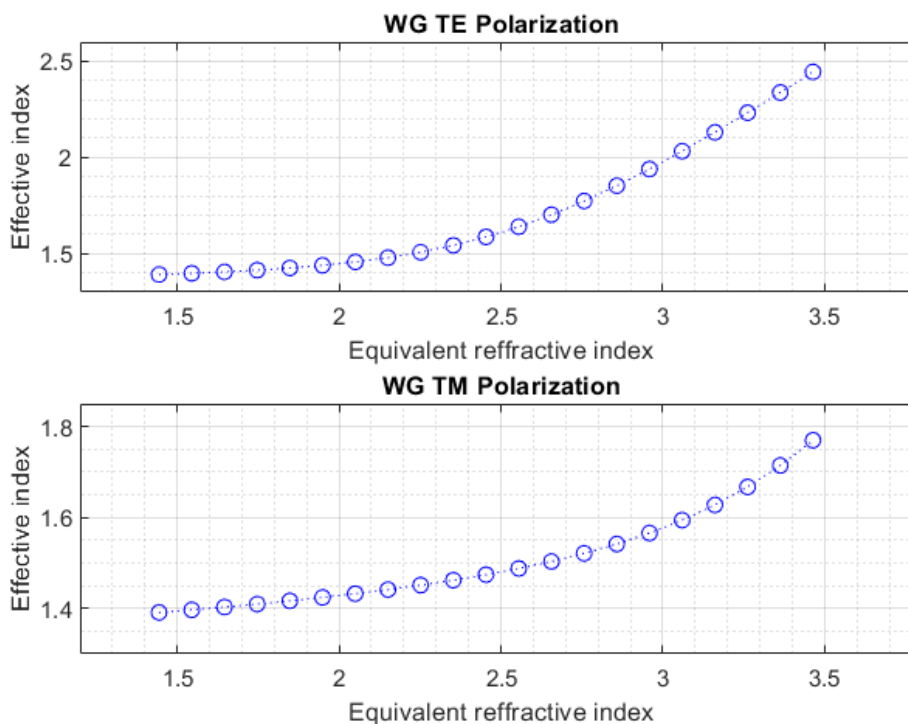


Fig. 39. Effective indices for a waveguide with the standard dimensions of the silicon but using other materials.

The structure would be similar to the device shown at the top of Fig. 40. Defining a structure with the adequate period it is possible to obtain the performance desired, as depicted at the bottom-right of Fig. 40.

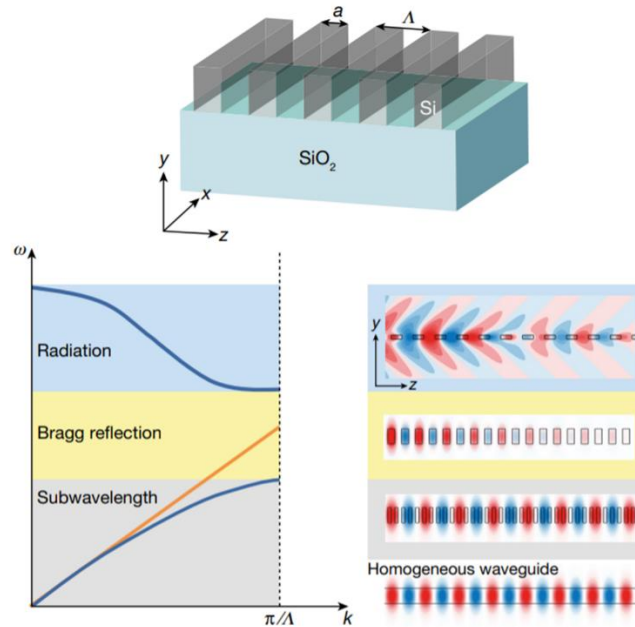


Fig. 40. Light propagation through a periodic dielectric structure [42].

All things considered, the configuration of the initial directional coupler can be good enough for high-power applications. However, an optimized subwavelength device could improve that results, thus it is a good starting point for a future work.

## Chapter 5. Conclusions and future work

### 5.1 Conclusions

Integrated photonics is positioning itself as one of the most powerful platforms to handle the problems arising from the growth of data consumption. In data networks, both user plane and control plane require smaller and faster equipment and. Considering the fast speed and large bandwidth offered by photonics systems, integrated photonics is presented as a solution. Moreover, most of the devices combine electronics and photonics. Thus, the using of silicon photonics is getting more and more relevant due to its CMOS compatibility.

In almost every photonic integrated circuit there are numerous directional couplers (or other kind of coupling structures, such as ring resonators). Therefore, the optimization of these devices is critical to achieve the best performance.

Throughout this work, the design and analysis of an asymmetrical directional coupler combining silicon, silicon nitride and GST has been done. Starting from the analysis of the current devices, from the simplest to the most complex one, we have created a device that meets the operational requirements needed for high-power transmission in silicon photonics. Simulations with RSoft software, including FemSIM or BeamPROP, have been performed to develop the design presented.

Considering the results presented in this work, the use of asymmetric directional couplers combining silicon and silicon nitride can be widely used for the high-power links in the photonic integrated chips of the future. The advantage of separating the control signal from the data signal can be exploited in circuits with a big number of structures, like the ones that are being designed nowadays. Furthermore, the addition of phase change materials, which are a hot topic in photonics due to their capabilities, make this kind of devices more and more interesting for the industry.

### 5.2 Future work

Despite the functionality of the asymmetric directional coupler is good enough, an optimization in terms of efficiency would be important for certain applications where the energy available is limited. To this end, some extra asymmetries can be added to the proposed directional coupler, similar to the results presented in [37]. The phase variations of the device can be corrected by means of extra sections of waveguides with different widths, optimizing the phase matching condition and obtaining a better coupling.

On the other hand, the total power coupling between the waveguides of the asymmetrical coupling is still not achieved. Maybe that is not possible due to the characteristics of the materials involved, but it could be analysed after the optimizations mentioned. Furthermore, the behaviour of the system can be confirmed with precise simulations using 3D FDTD tools, such as FullWAVE.



Then, GST has been widely used as active material and it is considered as one of the most powerful platforms to this end. However, if the final aim of the design is the fabrication of the device, there are still some issues to optimize about its use for in-plane all-optical switching [34]. The crystallization mentioned in the document should be improved, and it could be done by changing the pulses injected to the waveguides.

Finally, the last step of any design would be the fabrication of the device and its characterization. After a possible optimization of the performance using some of the techniques mentioned above it would be interesting to fabricate the chip, then doing the measurements, analysing the results and correlate the behaviour between the simulated and the experimental values.

## List of figures

Fig. 1. PON transceiver made by Bookham in 1993 [6].	3
Fig. 2. Forecast of silicon photonics from 2020 to 2026 [12].	5
Fig. 3. Bend radius, propagation loss, and window of transparency for SiN and SOI waveguides [17].	6
Fig. 4. Si <sub>3</sub> N <sub>4</sub> based passive devices [18]. (a) Side view of a bi-layer grating coupler. (b) Polarization rotator. (c) Polarization beam splitter from [21].	7
Fig. 5. Si <sub>3</sub> N <sub>4</sub> based active devices [18]. (a) Microscopic image of a microring modulator. (b) SEM image of a PZT-covered SiN waveguide. (c) Photodetector with graphene on the SiN waveguide. (d) SEM image of areas with and without graphene.	8
Fig. 6. Si <sub>3</sub> N <sub>4</sub> waveguide types, cross sections and SEM photographs [17].	9
Fig. 7. (a) Hybrid VO <sub>2</sub> /Si waveguide with a lateral Ti microheater[30]. (b) Si/Au/VO <sub>2</sub> all-optical modulator [26].	10
Fig. 8. Four all-optical switching cycles in a hybrid Silicon-GST waveguide. [34].	10
Fig. 9. Even mode and odd mode of supermodes theory [35].	11
Fig. 10. Design parameters of a directional coupler [35].	12
Fig. 11. Compact Silicon-on-Insulator polarization splitter [36].	12
Fig. 12. Schematic of broadband directional coupler [37].	13
Fig. 13. Silicon polarization beam splitter with an asymmetrical bent directional coupler. [38] (a) Image of the fabricated polarization beam splitter. (b) SEM picture for the bent directional coupler.	13
Fig. 14. Two configurations of broadband non-volatile photonic switches based on optical phase change materials. 1x2 switch at the top image. 2x2 switch at the bottom image [39].	14
Fig. 15. Si-SiN dual-layer directional coupler. [40]. (a) Schematic of the directional coupler. (b) Light intensity transfer between two layers.	14
Fig. 16. Top-view schematic of the proposed asymmetric Si-SiN directional coupler + phase change materials.	16
Fig. 17. Transversal section of the Si-SiN coupling region.	16
Fig. 18. Time diagram of the tasks carried out in this thesis.	17
Fig. 19. (a) Settings of the FemSIM simulation of the silicon waveguide. (b) Nonuniform mesh for the simulation of the silicon waveguide.	19
Fig. 20. Mode profile of the fundamental modes of the silicon waveguide obtained with FemSIM. (a) TE mode. (b) TM mode.	19
Fig. 21. Mode profile computed with FemSIM of the fundamental modes for a 500-nm-high and 1200-nm-wide silicon nitride waveguide. (a) TE mode. (b) TM mode.	20
Fig. 22. Settings of the MOST simulation tool for the sweep of the silicon nitride waveguide sizes.	21
Fig. 23. Results of the MOST simulation of the SiN waveguide in TE and TM polarizations.	22
Fig. 24. Even mode of the directional coupler with the identifier #1.	24
Fig. 25. Odd mode of the directional coupler with the identifier #1.	24



Fig. 26. Even mode (left) and odd mode (right) for the couplers with identifiers 2, 3, 4 and 5..	25
Fig. 27. Even mode (left) and odd mode (right) for the couplers with identifiers 6, 7, 8 and 9..	26
Fig. 28. Example of the input signal injected to the SiN waveguide of the directional coupler.	27
Fig. 29. Settings of the BeamPROP simulation. ....	28
Fig. 30. BeamPROP simulation of the structure with identifier 1.....	29
Fig. 31. Insertion loss vs. launched power in C-band for CW light. Two-photon absorption [41]. .....	29
Fig. 32. Two high-order modes of the structure with identifier 1. ....	30
Fig. 33. Simulation of the effective indices of the hybrid Si/GST structure for GST in amorphous state.....	30
Fig. 34. Simulation of the effective indices of the hybrid Si/GST structure for GST in crystalline state. ....	31
Fig. 35. Cross-section of the structure with identifier 1 changing the alignment of the waveguides.....	31
Fig. 36. BeamPROP simulation of the structure with identifier 1 changing the alignment of the waveguides.....	32
Fig. 37. Cross-section of a silicon slot waveguide. ....	32
Fig. 38. Effective indices of silicon waveguides with different width. ....	33
Fig. 39. Effective indices for a waveguide with the standard dimensions of the silicon but using other materials. ....	33
Fig. 40. Light propagation through a periodic dielectric structure [42]. ....	34

## References

- [1] R. Won, “Integrating silicon photonics,” *Nat. Photonics*, vol. 4, no. 8, pp. 498–499, 2010.
- [2] G. Lifante, “Introduction to Integrated Photonics,” *Integr. Photonics Fundam.*, pp. 1–23, 2005.
- [3] L. Thylén and L. Wosinski, “Integrated photonics in the 21st century,” *Photon. Res.*, vol. 2, no. 2, pp. 75–81, 2014.
- [4] L. Chrostowski and M. Hochberg, *Silicon Photonics Design: From Devices to Systems*. Cambridge: Cambridge University Press, 2015.
- [5] T. Aalto, M. Cherchi, M. Harjanne, F. Sun, and M. Kapulainen, *3Mm Silicon Photonics*. 2018.
- [6] A. Rickman, “The commercialization of silicon photonics,” *Nat. Photonics*, vol. 8, no. 8, pp. 579–582, 2014.
- [7] R. Soref and J. Lorenzo, “All-silicon active and passive guided-wave components for  $\lambda = 1.3$  and  $1.6 \mu\text{m}$ ,” *IEEE J. Quantum Electron.*, vol. 22, no. 6, pp. 873–879, 1986.
- [8] J. Chiles and S. Fathpour, “Silicon photonics beyond silicon-on-insulator,” 2017.
- [9] A. J. Shaikh and O. Sidek, “Making Silicon Emit Light Using Third Harmonic Generation,” *Procedia Eng.*, vol. 29, pp. 1456–1461, 2012.
- [10] C. Rios *et al.*, “Integrated all-photonic non-volatile multi-level memory,” *Nat. Photonics*, vol. 9, no. 11, pp. 725–732, 2015.
- [11] J. Parra, I. Olivares, A. Brimont, and P. Sanchis, “Toward Nonvolatile Switching in Silicon Photonic Devices,” *Laser Photon. Rev.*, vol. 15, no. 6, p. 2000501, Jun. 2021.
- [12] T. R. May, “Silicon Photonics 2021. More applications are emerging from silicon photonics,” *Mark. Technol. Rep.*, no. May, pp. 2020–2022, 2021.
- [13] R. Baets *et al.*, “Silicon photonics: Silicon nitride versus silicon-on-insulator,” in *2016 Optical Fiber Communications Conference and Exhibition (OFC)*, 2016, pp. 1–3.
- [14] R. G. Heideman *et al.*, “Large-scale integrated optics using TriPleX (TM) waveguide technology: from UV to IR,” *Appl. Phys. B-lasers Opt.*, vol. 7221, Feb. 2009.
- [15] I. Perez-Arjona, G. J. de Valcárcel, and E. Roldan, “Two-photon absorption,” *Rev. Mex. física*, vol. 49, pp. 92–101, 2003.
- [16] J. B. Khurgin, T. H. Stievater, M. W. Pruessner, and W. S. Rabinovich, “On the origin of the second-order nonlinearity in strained Si<sub>3</sub>N<sub>4</sub> structures,” *J. Opt. Soc. Am. B*, vol. 32, no. 12, pp. 2494–2499, 2015.
- [17] D. J. Blumenthal, R. Heideman, D. Geuzebroek, A. Leinse, and C. Roeloffzen, “Silicon Nitride in Silicon Photonics,” *Proc. IEEE*, vol. 106, no. 12, pp. 2209–2231, 2018.
- [18] T. Sharma *et al.*, “Review of Recent Progress on Silicon Nitride-Based Photonic Integrated Circuits,” *IEEE Access*, vol. 8, pp. 195436–195446, 2020.
- [19] J. C. C. Mak, Q. Wilmart, S. Olivier, S. Menezo, and J. K. S. Poon, “Silicon nitride-on-silicon bi-layer grating couplers designed by a global optimization method,” *Opt. Express*, vol. 26, no. 10, pp. 13656–13665, 2018.
- [20] M. Zadka, Y.-C. Chang, A. Mohanty, C. T. Phare, S. P. Roberts, and M. Lipson, “On-chip platform for a phased array with minimal beam divergence and wide field-of-view,” *Opt. Express*, vol. 26, no. 3, pp. 2528–2534, 2018.



- [21] X. Sun, J. Aitchison, and M. Mojahedi, “Realization of an ultra-compact polarization beam splitter using asymmetric MMI based on silicon nitride / silicon-on-insulator platform,” *Opt. Express*, vol. 25, p. 8296, Apr. 2017.
- [22] J. Wang, Z. Cheng, Z. Chen, J.-B. Xu, H. K. Tsang, and C. Shu, “Graphene photodetector integrated on silicon nitride waveguide,” *J. Appl. Phys.*, vol. 117, no. 14, p. 144504, Apr. 2015.
- [23] A. Z. Subramanian *et al.*, “Silicon and silicon nitride photonic circuits for spectroscopic sensing on-a-chip [Invited],” *Photonics Res.*, vol. 3, no. 5, pp. B47–B59, 2015.
- [24] C. Xiang *et al.*, “High-performance lasers for fully integrated silicon nitride photonics,” 2021.
- [25] A. Leinse, S. Zhang, and R. Heideman, “TriPleX: The versatile silicon nitride waveguide platform,” in *2016 Progress in Electromagnetic Research Symposium (PIERS)*, 2016, p. 67.
- [26] K. J. Miller, R. F. Haglund, and S. M. Weiss, “Optical phase change materials in integrated silicon photonic devices: review,” *Opt. Mater. Express*, vol. 8, no. 8, p. 2415, 2018.
- [27] Y. Zhang *et al.*, “Broadband transparent optical phase change materials for high-performance nonvolatile photonics,” *Nat. Commun.*, vol. 10, no. 1, pp. 1–9, 2019.
- [28] W. H. P. Pernice and H. Bhaskaran, “Photonic non-volatile memories using phase change materials,” *Appl. Phys. Lett.*, vol. 101, no. 17, 2012.
- [29] E. Kuramochi and M. Notomi, “Optical memory: Phase-change memory,” *Nat. Photonics*, vol. 9, no. 11, pp. 712–714, 2015.
- [30] I. Olivares *et al.*, “Optical switching in hybrid VO<sub>2</sub>/Si waveguides thermally triggered by lateral microheaters,” *Opt. Express*, vol. 26, no. 10, p. 12387, 2018.
- [31] M. R. Otto *et al.*, “How optical excitation controls the structure and properties of vanadium dioxide,” *Proc. Natl. Acad. Sci. U. S. A.*, vol. 116, no. 2, pp. 450–455, 2019.
- [32] H. M. K. Wong *et al.*, “Broadband, Integrated, Micron-Scale, All-Optical Si<sub>3</sub>N<sub>4</sub>/VO<sub>2</sub> Modulators with pJ Switching Energy,” *ACS Photonics*, vol. 6, no. 11, pp. 2734–2740, 2019.
- [33] A. Joushaghani, J. Jeong, S. Paradis, D. Alain, J. Stewart Aitchison, and J. K. S. Poon, “Wavelength-size hybrid Si-VO<sub>2</sub> waveguide electroabsorption optical switches and photodetectors,” *Opt. Express*, vol. 23, no. 3, p. 3657, 2015.
- [34] A. Santomé, H. Urgelles-Pérez, J. Parra, and P. Sanchis, “High-performance optical switches based on GST/Si waveguides,” *Spintron. Photonics, Phononics or Magneto-Optics Onl. Int. Conf. (SPPM 2021)*, pp. 35-35., 2021.
- [35] P. Sanchis, “Basic structures in photonic integrated circuits,” *Nanophotonics. MUTSRC-UPV*, 2020.
- [36] I. Kiyat, A. Aydinli, and N. Dagli, “A compact silicon-on-insulator polarization splitter,” *IEEE Photonics Technol. Lett.*, vol. 17, no. 1, pp. 100–102, 2005.
- [37] Z. Lu *et al.*, “Broadband silicon photonic directional coupler using asymmetric-waveguide based phase control,” *Opt. Express*, vol. 23, no. 3, pp. 3795–3808, 2015.
- [38] J. Wang, D. Liang, Y. Tang, D. Dai, and J. E. Bowers, “Realization of an ultra-short silicon polarization beam splitter with an asymmetrical bent directional coupler,” *Opt. Lett.*, vol. 38, no. 1, pp. 4–6, 2013.
- [39] Q. Zhang, Y. Zhang, J. Li, R. Soref, T. Gu, and J. Hu, “Broadband nonvolatile photonic



switching based on optical phase change materials: beyond the classical figure-of-merit,” *Opt. Lett.*, vol. 43, no. 1, p. 94, 2018.

- [40] J. Ma *et al.*, “A SiN-Si Dual-layer Directional Coupler,” in *2020 Asia Communications and Photonics Conference (ACP) and International Conference on Information Photonics and Optical Communications (IPOC)*, 2020, pp. 1–3.
- [41] G. U.- Imec, “Origin of nonlinear loss in silicon waveguides,” *SM2J.3*, 2021.
- [42] P. Cheben, R. Halir, J. H. Schmid, H. A. Atwater, and D. R. Smith, “Subwavelength integrated photonics,” *Nature*, vol. 560, no. 7720, pp. 565–572, 2018.